Annual Reviews in Control 54 (2022) 386–408

Contents lists available at ScienceDirect

Annual Reviews in Control

journal homepage: www.elsevier.com/locate/arcontrol

Review

Fractional cyber-neural systems — A brief survey☆

Emily Reed [a,*,1], Sarthak Chatterjee [b,1], Guilherme Ramos [c,1], Paul Bogdan [a], Sérgio Pequito [d]

[a] Ming Hsieh Department of Electrical and Computer Engineering, University of Southern California, Los Angeles, CA, USA
[b] Department of Electrical, Computer, and Systems Engineering, Rensselaer Polytechnic Institute, Troy, NY, USA
[c] LASIGE, Departamento de Informática, Faculdade de Ciências, Universidade de Lisboa, Portugal
[d] Delft Center for Systems and Control, Delft University of Technology, Delft, The Netherlands

ARTICLE INFO

Keywords:
Fractional-order systems
Cyber-neural systems
Neurotechnology

ABSTRACT

Neurotechnology has made great strides in the last 20 years. However, we still have a long way to go to commercialize many of these technologies as we lack a unified framework to study cyber-neural systems (CNS) that bring the hardware, software, and the neural system together. Dynamical systems play a key role in developing these technologies as they capture different aspects of the brain and provide insight into their function. Converging evidence suggests that fractional-order dynamical systems are advantageous in modeling neural systems because of their compact representation and accuracy in capturing the long-range memory exhibited in neural behavior. In this brief survey, we provide an overview of fractional CNS that entails fractional-order systems in the context of CNS. In particular, we introduce basic definitions required for the analysis and synthesis of fractional CNS, encompassing system identification, state estimation, and closed-loop control. Additionally, we provide an illustration of some applications in the context of CNS and draw some possible future research directions. Advancements in these three areas will be critical in developing the next generation of CNS, which will, ultimately, improve people's quality of life.

1. Introduction

We have witnessed an increase in the popularity of neurotechnology, which in part has been propelled by several Silicon Valley companies such as NeuraLink (Regalado, 2020) (founded by Elon Musk), Google, and Facebook, just to mention a few. This trend is now emerging in Europe as well with a variety of start-up companies across different countries. Yet, we have a long path going forward to commercialize these devices to a clinical domain (Carmena, Sajda, & Robinson, 2019; Chavarriaga, 2020; Lewis, 2020). Among the different neurotechnologies, the one experiencing the biggest growth is the neurostimulation device, which assesses the neural activity (e.g., by tracking the change in electrical potential) and injects a timely stimulus (e.g., current from electrical neurostimulation devices) that aims to disrupt such activity (Rodgers, 2020). These devices consist of tightly integrated hardware and software components that monitor and regulate the dynamics of the neural system. Together, the intertwined behavior generated by the interaction of the hardware/software and the neural systems form the so-called cyber-neural system (CNS).

Neural systems, such as the brain, generally exhibit quite diverse activity patterns across subjects under different operational setups (Bargmann et al., 2014). Therefore, it is important to develop tools to translate these behaviors to enable CNS to become tomorrow's reality. Many efforts world-wide, such as the Brain Initiative (Insel, Landis, & Collins, 2013), Human Connectome Project (Van Essen et al., 2013), and Human Brain Project (Markram, 2012), have sought to understand the brain in health and disease. Additionally, they also seek to provide new insights into how to "reverse-engineer the brain," a grand challenge deemed by the National Academy of Engineering (NAE, 2022). Consequently, it is imperative to establish a unified robust framework to understand and regulate brain activity across individuals and regimes (both healthy as well as diseased/disordered) (LeDoux,

☆ This work was supported by FCT through the LASIGE Research Unit ref. UIDB/00408/2020 and ref. UIDP/00408/2020, National Science Foundation GRFP DGE-1842487, Career Award CPS/CNS-1453860, CCF-1837131, MCB-1936775, CNS-1932620, CMMI-1936624, CMMI 1936578, the University of Southern California Annenberg Fellowship, USC WiSE Top-Off Fellowship, the DARPA Young Faculty Award and DARPA Director Award N66001-17-1-4044. The views, opinions, and/or findings contained in this article are those of the authors and should not be interpreted as representing the official views or policies, either expressed or implied by the Defense Advanced Research Projects Agency, the Department of Defense, or the National Science Foundation.

* Corresponding author.
E-mail addresses: emilyree@usc.edu (E. Reed), sarthak.chatterjee@merck.com (S. Chatterjee), ghramos@fc.ul.pt (G. Ramos), pbogdan@usc.edu (P. Bogdan), Sergio.Pequito@tudelft.nl (S. Pequito).

[1] The authors contributed equally.

https://doi.org/10.1016/j.arcontrol.2022.06.002
Received 15 December 2021; Accepted 3 June 2022
Available online 6 July 2022

1998; Markram, 2012; Van Essen et al., 2013). Ultimately, this understanding will lead to an improvement in treatments and therapies for diseased patients, which will enhance their overall quality of life.

Fortunately, each year, we get new insights and a better understanding about life-changing neurological diseases. These advances in understanding neural systems and in providing adequate treatment for these diseases have been mostly achieved with the help of technology that can measure and record neural activity (Fairclough & Lotte, 2020). Scientists and researchers use these measurements of the brain's activity to create models of the brain.

There are different methods to analyze and design cyber-neural systems. One useful tool in modeling is a dynamical network system (Bassett & Sporns, 2017). For example, Presigny and Fallani (2021) provide an overview of the recent advances in modeling the multiscale behavior of the brain using dynamical networks. These models have allowed researchers to draw conclusions regarding the brain's topology and function. While many studies have used linear dynamical systems to model neural behavior (Ashourvan et al., 2020; Li, Inati, Zaghloul, & Sarma, 2017; Pequito, Ashourvan, Bassett, Litt, & Pappas, 2017), these models are unable to capture the nonlinear and non-Markovian behavior exhibited in the brain (Shlesinger, Zaslavsky, & Klafter, 1993; West, 2016; Zhang & Chen, 2012). On the other hand, several studies have used more complex nonlinear models; however, these models are not easy to interpret and explain in the context of brain dynamics (Bonilla, Rivero, Rodríguez-Germá, & Trujillo, 2007; West, Turalska, & Grigolini, 2015).

Fractional-order dynamical systems, which originated in physics and economics and quickly found their way into engineering applications (Baleanu, Diethelm, Scalas, & Trujillo, 2012; Kilbas, Srivastava, & Trujillo, 2006; Petráš, 2011; Podlubny, 1998; Sabatier, Agrawal, & Machado, 2007; Valério, Trujillo, Rivero, Machado, & Baleanu, 2013; West, 2014), are appealing mainly due to their representation as a compact spatiotemporal dynamical system with two easy-to-interpret sets of parameters, namely the *fractional-order coefficients* and the *spatial matrix*. Fractional-order coefficients capture the long-range memory in the dynamics of each state variable of the system, and the spatial matrix represents the spatial coupling between different state variables.

Fractional-order systems provide an efficient way to model many different systems, including viral spreading (Oustaloup, Levron, Victor, & Dugard, 2021), heat flux (Battaglia, Le Lay, Batsale, Oustaloup, & Cois, 2000; Victor, Melchior, Malti, & Oustaloup, 2016), the human bronchus (Duhé, Victor, Melchior, Abdelmounen, & Roubertie, 2022), human muscles (Melchior, Pellet, Petit, Cabelguen, & Oustaloup, 2012), the nervous system (Werner, 2010), electrocardiogram signals (Turcott & Teich, 1996), brain activity (Lundstrom, Higgs, Spain, & Fairhall, 2008; Teich, Heneghan, Lowen, Ozaki, & Kaplan, 1997; Thurner, Windischberger, Moser, Walla, & Barth, 2003), and anomalous diffusion (Chen, Sun, Zhang, & Korošak, 2010). Furthermore, fractional-order systems have been used in domains as disparate as biological networks (West, Turalska, & Grigolini, 2016), cyber–physical systems (Xue & Bogdan, 2017; Xue, Rodriguez & Bogdan, 2016), nanotechnology (Baleanu et al., 2010), finance (Scalas, Gorenflo, & Mainardi, 2000), quantum mechanics (Shahin, Ahmed, & Omar, 2009), phasor measurement unit (PMU) data in the power grid (Shalalfeh, Bogdan, & Jonckheere, 2020), and networked control systems (Cao, Li, Ren, & Chen, 2009; Chen, 2010; Ren & Cao, 2011), to mention a few.

In this brief survey, we focus our attention on neural behavior, which can be accurately represented by fractional-order systems (Baleanu, Machado, & Luo, 2011; Lundstrom et al., 2008; Moon, 2008; Teich et al., 1997; Thurner et al., 2003; Werner, 2010; West et al., 2016). Fractional-order systems have also been explored in the context of neurophysiological networks constructed from electroencephalographic (EEG), electrocorticographic (ECoG), or blood-oxygen-level-dependent (BOLD) data (Chatterjee, Romero, Ashourvan, & Pequito, 2020; Magin, 2006).

Furthermore, we provide an overview of the work that has been done on controlling, estimating, and predicting neural dynamical systems modeled using fractional-order dynamics both in the continuous-time and discrete-time domains, towards the next generation of CNS, which are important for advancing the understanding of neural systems as well as treatments for neurological diseases. Specifically, the focus of our brief survey is threefold:

- **Control:** We review different methods to control fractional-order systems, including a few previously presented methods in Efe (2011). The work in Birs, Muresan, Nascu, and Ionescu (2019) presents a survey of recent advances in fractional-order control for time delay systems, and the works in Chen, Petras, and Xue (2009), Matušů (2011) provide overviews of the application of fractional calculus to control theory. In this paper, we review proportional–integral control, sliding mode control, backstepping control, adaptive control, optimal control, and model predictive control for fractional-order systems. Control of fractional-order systems is important to study so as to develop methods and therapies to mitigate and potentially eliminate diseases in the brain.
- **System Identification:** System identification of continuous-time fractional-order systems has been examined for non-commensurate (i.e., fractional-order coefficients are non-uniform across states) systems (Mayoufi, Victor, Chetoui, Malti, & Aoun, 2021; Victor, Malti, Garnier, & Oustaloup, 2013), for commensurate-order systems with time delays (Narang, Shah, & Chen, 2011), for thermal systems modeled as fractional linear systems (Gabano, Poinot, & Kanoun, 2011), and for lithium-ion batteries using a nonlinear optimization least squares method (Eddine, Huard, Gabano, & Poinot, 2018). For discrete-time fractional-order systems, system identification has been studied to determine the best estimate of the fractional-order system parameters with unknown inputs (Gupta, Pequito, & Bogdan, 2018a, 2018b) and when the data is only partially observable (Gupta, Pequito, & Bogdan, 2019) as well as with non-asymptotic finite-sample complexity guarantees (Chatterjee & Pequito, 2022). In what follows, the focus will be on estimating the parameters of fractional-order systems from brain measurements, such as electroencephalography (EEG) and electrocorticography (ECoG). Therefore, we focus on system identification methods for discrete-time fractional-order systems, which is a necessary step in understanding the intricacies of the brain.
- **Estimation:** We discuss the methods for estimating and predicting the state of fractional-order systems (Chatterjee & Pequito, 2019; Miljković, Popović, Djordjević, Konstantinović, & Šekara, 2017; Najar, Abdelkrim, Abdelhamid, & Mohamed, 2009; Sabatier, Farges, Merveillaut, & Feneteau, 2012; Safarinejadian, Asad, & Sadeghi, 2016; Safarinejadian, Kianpour, & Asad, 2018; Sierociuk & Dzieliński, 2006). This problem is important in anticipating and mitigating irregular brain behavior such as an oncoming seizure. Chatterjee, Alessandretti, Aguiar, and Pequito (2021) proposed the design of a minimum-energy estimation framework for discrete-time fractional-order networks, where they assume that the state and output equations are affected by an additive disturbance and noise, respectively, that are deterministic, bounded, and unknown. First proposed by Mortensen (Mortensen, 1968), and later refined by Hijab (Hijab, 1980), minimum-energy estimators produce an estimate of the system state that is the "most consistent" with the dynamics and the measurement updates of the system (Aguiar & Hespanha, 2006; Alessandretti, Aguiar, Hespanha, & Valigi, 2011; Bonnabel & Slotine, 2015; Buchstaller, Liu, & French, 2020; Fagnani & Willems, 1997; Fleming, 1997; Ha & Aguiar, 2018; Haring & Johansen, 2020; Hassani, Aguiar, Athans, & Pascoal, 2009; Krener, 2003; Pequito, Aguiar, & Gomes, 2009; Swerling, 1971; Willems, 2004).

Section 2 overviews continuous-time fractional-order dynamics. Section 3 summarizes discrete-time fractional-order dynamics. Section 4 presents the results on the stability of fractional-order systems. Section 5 provides a summary of the work on controllability and observability of fractional-order systems. Section 6 summarizes the work on proportional–integral–derivative controllers for fractional-order dynamical systems. Section 7 reviews sliding mode control for fractional-order systems. Section 8 outlines the procedure for constructing a backstepping controller for fractional-order systems. Section 9 summarizes adaptive control for fractional-order systems. Section 10 discusses the methods for performing system identification on fractional-order systems. Section 11 overviews the techniques for state estimation of fractional-order systems, including the method known as minimum-energy state estimation. Section 12 presents fractional optimal control for continuous-time fractional-order systems. Section 13 gives a background on model predictive control for fractional-order systems. Section 14 summarizes simulation results pertaining to system identification, state estimation, and closed-loop control of fractional cyber-neural systems. Finally, Section 15 presents possible directions for future research.

2. Continuous-time fractional-order systems

To model, analyze, and control fractional-order dynamics, we first provide an overview of both continuous-time and discrete-time fractional-order systems. We start by introducing the fractional-order system in continuous-time (Kilbas & Trujillo, 2001, 2002).

Riemann–Liouville and Caputo proposed the two commonly used definitions of fractional-order differintegration. However, Riemann–Liouville's definition poses restrictions on the interpretation of the initial conditions (Podlubny, 1999). Caputo's definition may require special attention regarding the initialization scheme (Jean-Claude, Nezha, & Alain, 2013; Trigeassou & Maamri, 2011). Regardless, the latter has been widely used in control systems engineering, and it is the following:

$$\Delta^{\alpha}\sigma(t) = \frac{1}{\Gamma(m-\alpha)}\int_0^t \frac{\Delta^m\sigma(\tau)}{(t-\tau)^{\alpha+1-m}}\,\mathrm{d}\tau, \tag{1}$$

where Δ^{α} is the fractional differintegration operator, $\alpha \in \mathbb{R}^+$ is the fractional-order exponent, and $\Gamma(\alpha) = \int_0^{\infty} e^{-t}t^{\alpha-1}\,\mathrm{d}t$ is the Gamma function (Baleanu et al., 2012). Given the definition in (1), let $m \in \mathbb{Z}$ with $m-1 < \alpha < m$. For an m satisfying the previous relation, the α order derivative of a function of time, $\sigma(t)$, has the following Laplace transform:

$$\int_0^{\infty} e^{-st}\Delta^{\alpha}\sigma(t)\,\mathrm{d}t = s^{\alpha}S(s) - \sum_{k=0}^{m-1} s^{\alpha-k-1}\Delta^{k}\sigma(0), \tag{2}$$

where $S(s) = \int_0^{\infty} e^{-st}\sigma(t)\,\mathrm{d}t$.

If a fractional-order system is initially in a resting state (i.e., the initial conditions are zero), then the operator Δ^{α} acting in the time domain has a counterpart s^{α} in the s-domain. In this case, we can describe the transfer function of a fractional-order system by a fractional-order differential equation

$$\begin{aligned}&\left(a_n\Delta^{\alpha_n} + a_{n-1}\Delta^{\alpha_{n-1}} + \cdots + a_1\Delta^{\alpha_1} + a_0\right)y(t)\\ &\quad = \left(b_m\Delta^{\beta_m} + b_{m-1}\Delta^{\beta_{m-1}} + \cdots + b_1\Delta^{\beta_1} + b_0\right)u(t),\end{aligned} \tag{3}$$

which we can rewrite as

$$\frac{Y(s)}{U(s)} = \frac{a_n s^{\alpha_n} + a_{n-1}s^{\alpha_{n-1}} + \cdots + a_1 s^{\alpha_1} + a_0}{b_m s^{\beta_m} + b_{m-1}s^{\beta_{m-1}} + \cdots + b_1 s^{\beta_1} + b_0}, \tag{4}$$

where $a_k, b_k \in \mathbb{R}$ and $\alpha_k, \beta_k \in \mathbb{R}^+$.

Therefore, we can write an affine and fractional-order nonlinear non-commensurate system as

$$\Delta^{\alpha}x(t) = \mathbf{f}(x(t)) + \mathbf{g}(x(t))u(t) \tag{5}$$

where $\alpha \in \mathbb{R}^n$, $u(t) \in \mathbb{R}^m$ is the control input, and $\mathbf{f}$ and $\mathbf{g} \neq 0$ are the vector functions of the system-state $x(t) \in \mathbb{R}^n$. A special case of Eq. (5) is given as a state-space representation

$$\begin{aligned}\Delta^{\alpha}x(t) &= Ax(t) + Bu(t)\\ y(t) &= Cx(t) + Du(t),\end{aligned} \tag{6}$$

where $x(t) \in \mathbb{R}^n$ and $\alpha \in \mathbb{R}^n$. Eq. (6) is referred to as the linear non-commensurate fractional-order system. The transfer function, which characterizes the relationship between $Y(s)$ and $U(s)$, where $Y(s)$ and $U(s)$ are the Laplace transforms of the output and input, respectively, of the state-space system in (6), is given as

$$H(s) = C\left(s^{\alpha}I - A\right)^{-1}B + D. \tag{7}$$

Therefore, we have the following solution for the homogeneous case (i.e., $u(t) = 0$)

$$x(t) = E_{\alpha}\left(At^{\alpha}\right)x(0) = \Phi(t)x(0), \tag{8}$$

where $E_{\alpha}\left(At^{\alpha}\right)$ is the *Mittag-Leffler function* (Oldham & Spanier, 1974) defined as

$$\Phi(t) \equiv E_{\alpha}\left(At^{\alpha}\right) = \sum_{k=0}^{\infty}\left(\frac{\left(At^{\alpha}\right)^k}{\Gamma(1+\alpha k)}\right).$$

Therefore, we can write the solution of the fractional state equation and the output equation in (6) as

$$y(t) = C\Phi\left(t-t_0\right)x\left(t_0\right) + C\int_0^t \Phi(t-\tau)Bu(\tau)\,\mathrm{d}\tau + Du(t).$$

Despite the fact that real-world systems have continuous-time signals in nature, in reality, we measure and control these systems using digitized technologies, which motivates the study of discrete-time fractional-order systems (Caponetto, 2010; Goodrich & Peterson, 2015; Mahmoud, 2012). Subsequently, we now introduce the discrete-time description of the fractional-order dynamics.

3. Discrete-time fractional-order systems

In what follows next, we briefly introduce discrete-time fractional-order system models. We start by introducing the Grünwald–Letnikov derivative as

$$\Delta^{\alpha}\sigma(t) = \lim_{h\to 0}\frac{1}{h^{\alpha}}\sum_{j=0}^{k}(-1)^j\binom{\alpha}{j}\sigma(t-jh), \tag{9}$$

where Δ^{α} is the fractional differintegration operator and $\alpha \in \mathbb{R}^+$ is the fractional-order exponent (Podlubny, 1999). If $\alpha > 0$, $m = \lceil\alpha\rceil$, and σ is continuously differentiable at least m times, then, for $t \in (a, b]$, the Grünwald–Letnikov definition is equivalent to the Riemann–Liouville definition (Diethelm, 2010, Theorem 2.25). Subsequently, it is possible to consider the Grünwald–Letnikov difference equation (or, simply speaking, the discrete derivative) as follows (Dzielinski & Sierociuk, 2005)

$$\Delta^{\alpha}\sigma[k] = \frac{1}{h^{\alpha}}\sum_{j=0}^{k}(-1)^j\binom{\alpha}{j}\sigma[k-j], \tag{10}$$

where $\alpha \in \mathbb{R}$ is the fractional-order exponent and h is a sampling time and $k \in \mathbb{N}$ is the sample number for which the derivative is calculated. In what follows, and without loss of generality, we consider unitary sampling time, i.e., we consider $h = 1$.

A discrete-time linear fractional-order system (DTLFOS) is described as follows:

$$\Delta^{\alpha}x[k+1] = Ax[k] + Bu[k] + w[k], \tag{11}$$

where $x[k] \in \mathbb{R}^n$ is the state for time step $k \in \mathbb{N}$, $A \in \mathbb{R}^{n\times n}$ is the state coupling matrix and $\alpha \in (\mathbb{R}^n)^+$ is the vector of fractional-order coefficients. The signal $u[k] \in \mathbb{R}^{n_u}$ denotes the input corresponding to the actuation signal, and the matrix $B \in \mathbb{R}^{n\times n_u}$ is the input matrix that

scales the actuation signal. The term $w[k] \in \mathbb{R}^n$ denotes the process noise or additive disturbance, whose stochastic characterization (or the lack thereof) will be clear from the context in which these systems are being used. These models are similar to classical discrete-time linear time-invariant system models with the exception of the inclusion of the Grünwald–Letnikov fractional derivative, whose expansion and discretization for the ith state, $1 \leq i \leq n$, can be expressed as (Dzielinski & Sierociuk, 2005; Vinagre, Podlubny, Hernandez, & Feliu, 2000)

$$\Delta^{\alpha_i} x_i[k] = \sum_{j=0}^{k} \psi(\alpha_i, j) x_i[k-j], \tag{12}$$

where α_i is the fractional-order coefficient corresponding to the state i and

$$\psi(\alpha_i, j) = \frac{\Gamma(j-\alpha_i)}{\Gamma(-\alpha_i)\Gamma(j+1)}. \tag{13}$$

Simply put, larger values of the fractional-order coefficients imply a lower dependency on the previous data from that state (i.e., a faster decay of the weights used as linear combination of previous data).

We now review some essential theory for fractional-order systems, including an approximation of (11) with $u[k] = 0$ for all $k \in \mathbb{N}$ as an LTI system. Using the expansion of the Grünwald–Letnikov derivative in (12), we have

$$\begin{aligned}
\Delta^{\alpha} x[k] &= \begin{bmatrix} \Delta^{\alpha_1} x_1[k] \\ \vdots \\ \Delta^{\alpha_n} x_n[k] \end{bmatrix} = \begin{bmatrix} \sum_{j=0}^{k} \psi(\alpha_1, j) x_1[k-j] \\ \vdots \\ \sum_{j=0}^{k} \psi(\alpha_n, j) x_n[k-j] \end{bmatrix} \\
&= \sum_{j=0}^{k} \underbrace{\begin{bmatrix} \psi(\alpha_1, j) & \dots & 0 \\ \vdots & \ddots & \vdots \\ 0 & \dots & \psi(\alpha_n, j) \end{bmatrix}}_{D(\alpha, j)} \begin{bmatrix} x_1[k-j] \\ \vdots \\ x_n[k-j] \end{bmatrix} \\
&= \sum_{j=0}^{k} D(\alpha, j) x[k-j].
\end{aligned} \tag{14}$$

The above formulation distinctly highlights one of the main peculiarities of DTLFOS in that the fractional derivative $\Delta^{\alpha} x[k]$ is a weighted linear combination of not just the previous state but of every single state up to the current one, with the weights given by (13) following a power-law decay.

Plugging (14) into the DTLFOS formulation (11) with $u[k] = 0$ for all $k \in \mathbb{N}$, we have

$$\sum_{j=0}^{k+1} D(\alpha, j) x[k+1-j] = Ax[k] + w[k], \tag{15}$$

or, equivalently,

$$D(\alpha, 0) x[k+1] = -\sum_{j=1}^{k+1} D(\alpha, j) x[k+1-j] + Ax[k] + w[k], \tag{16}$$

which leads to

$$x[k+1] = -\sum_{j=0}^{k} D(\alpha, j+1) x[k-j] + Ax[k] + w[k], \tag{17}$$

since $D(\alpha, 0) = I_n$, where I_n is the $n \times n$ identity matrix. Alternatively, (17) can be written as

$$\begin{aligned}
x[k+1] &= \sum_{j=0}^{k} A_j x[k-j] + w[k] \\
x[0] &= x_0,
\end{aligned} \tag{18}$$

where

$$A_j = \begin{cases} A - \operatorname{diag}(\psi(\alpha_1, 1), \dots, \psi(\alpha_n, 1)) & \text{if } j = 0 \\ -D(\alpha, j+1) & \text{if } j \geq 1. \end{cases} \tag{19}$$

4. Stability

Stability can be described as the behavior of the state of a system after a reasonable amount of time. While there are different notions of stability, in effect, a system is stable if the behavior of the system is bounded. The prior literature describes conditions for continuous-time fractional-order systems (Benzaouia, Hmamed, Mesquine, Benhayoun, & Tadeo, 2014; Li, Chen, & Podlubny, 2009; Monje, Chen, Vinagre, Xue, & Feliu-Batlle, 2010) and for single-input single-output continuous-time *commensurate* systems (Dastjerdi, Vinagre, Chen, & HosseinNia, 2019). Li, Chen, and Podlubny (2010) provide the generalized Mittag–Leffler stability conditions of continuous-time fractional-order systems using the Lyapunov direct method. In what follows, we summarize the stability conditions for continuous-time commensurate linear fractional-order systems. Let $\sigma(A) = \{\lambda_1, \dots, \lambda_n\}$ be the spectrum (set of eigenvalues) of A. We say that the commensurate system in (6) is stable if

$$\arg(\lambda_i) > \alpha \frac{\pi}{2}, \quad \text{for all } i = 1, \dots, n, \tag{20}$$

where $\arg(z)$, in the complex plane, is the 2D polar angle φ from the positive real axis to the vector representing z, and $0 < \alpha < 2$ (Rivero, Rogosin, Tenreiro Machado, & Trujillo, 2013). In the case of the transfer function in (7), we have that $\sigma(A)$ corresponds to the poles of the system, and the previous stability condition of (20) also applies. Notice that, in the integer order case ($\alpha = 1$), the stability condition of (20) describes the open left half s-plane. For a more detailed discussion on the stability of continuous-time systems, we refer the reader to Chen, Ahn, and Podlubny (2005), Matignon (1996), Ortigueira (2000).

For discrete-time fractional-order systems, the authors of Dzieliński and Sierociuk (2008) leverage an infinite dimensional representation of truncated discrete-time linear fractional-order systems (i.e., with finite memory) to give conservative sufficient conditions for stability. While the work in Busłowicz and Ruszewski (2013) does provide necessary and sufficient conditions for practical and asymptotic stability of discrete-time fractional-order systems, they only consider commensurate-order systems. Recent work has introduced stability conditions for multivariate discrete-time linear fractional-order systems with arbitrary fractional coefficients and leverages these conditions to study the stability of a real-world EEG cognitive motor data set modeled as a discrete-time fractional-order system and to provide evidence of its relevance in the context of cognitive motor control (Reed, Bogdan, & Pequito, 2021).

That said, a simple to state necessary and sufficient condition like (20) for both continuous and discrete-time non-commensurate systems is still missing. This limits the capability to assess the stability of such systems and their applicability in the context of neural systems and possibly some neurological diseases, such as epilepsy.

5. Controllability and observability

Controllability is a prerequisite in the ability to manipulate a system state to zero in a finite amount of time. On the other hand, observability is necessary to obtain a complete picture of the system on the whole. For continuous-time systems, Matignon and d'Andréa Novel (1996) give results on the controllability and observability of finite-dimensional continuous-time fractional-order systems. Balachandran et al. (2013) give a comprehensive overview of the conditions for controllability and observability of continuous-time linear fractional-order systems. Similarly, Guermah, Djennoune, and Bettayeb (2008) provide these results for discrete-time linear fractional-order systems. The work in Mozyrska and Pawłuszewicz (2012) derives the conditions for controllability and observability of finite memory discrete-time fractional-order systems.

Previous work has examined the design of controllable networks exhibiting discrete-time linear fractional-order dynamics using energy-based methods (Kyriakis, Pequito, & Bogdan, 2020) and by maximizing

the rank of the controllability matrix through a greedy algorithm (Cao, Ramos, Bogdan, & Pequito, 2019). Similarly, there has been work in selecting the minimal number of EEG sensors to achieve observability for discrete-time fractional-order systems (Gupta et al., 2018a; Pequito, Bogdan, & Pappas, 2015; Tzoumas, Xue, Pequito, Bogdan, & Pappas, 2018; Xue, Pequito, Coelho, Bogdan & Pappas, 2016).

A system is *controllable* if there exists a control input such that the final state can be driven to zero in a finite amount of time. In particular, for continuous-time linear fractional-order systems modeled by (6), the system is controllable on $[t_0, t_1]$ if for every pair of vectors $x(t_0), x(t_1) \in \mathbb{R}^n$, there is a control $u(t) \in L^2([t_0, t_1], \mathbb{R}^m)$ such that the solution $x(t)$ of (6) which satisfies $x(t_0) = x_0$ also satisfies $x(t_1) = x_1$, where $L^2([t_0, t_1], \mathbb{R}^m)$ is the space of all square integrable $\mathbb{R}^m$ valued measureable functions defined on $[t_0, t_1]$. Thus, we say that (6) is controllable on $[t_0, t_1]$ if and only if the controllability Gramian matrix

$$\int_{t_0}^{t_1} (t_1 - \tau)^{\alpha-1} E_{\alpha,\alpha}(A(t_1 - \tau)^\alpha) B B^\intercal E_{\alpha,\alpha}(A^\intercal (t_1 - \tau)^\alpha)\, \mathrm{d}\tau$$

is positive definite for some $t_1 > t_0$ (Balachandran et al., 2013, Theorem 3).

For discrete-time linear fractional-order system modeled by (11), the system is controllable if there exists a control sequence $\{\mathbf{u}[0], \dots, \mathbf{u}[T-1]\}$ such that $\mathbf{x}[T] = \mathbf{0}$ from any initial state $\mathbf{x}[0] \in \mathbb{R}^n$ in a finite time (Guermah et al., 2008). To present the conditions for controllability and observability for discrete-time fractional-order systems, we first start by noticing that the discrete-time linear fractional-order system (11) can be re-written as (Gupta et al., 2018a, Lemma 2):

$$x[k] = G_k x[0], \tag{21}$$

where

$$G_k = \begin{cases} I_n, & k = 0 \\ \sum_{j=0}^{k-1} A_j G_{k-1-j}, & k \geq 1 \end{cases} \tag{22}$$

with $A_0 = A - D(\alpha, 1)$, $A_j = -D(\alpha, j+1)$, for $j \geq 1$, and

$$D(\alpha, j) = \begin{bmatrix} \psi(\alpha_1, j) & 0 & \dots & 0 \\ 0 & \psi(\alpha_2, j) & \dots & 0 \\ 0 & \vdots & \ddots & 0 \\ 0 & 0 & \dots & \psi(\alpha_n, j) \end{bmatrix}. \tag{23}$$

The linear discrete-time fractional-order system modeled by (11) is controllable if and only if there exists a finite time K such that $\mathrm{rank}(W_c(0, K)) = n$, where $W_c(0, K) = G_K^{-1} \sum_{j=0}^{K-1} G_j B B^\intercal G_j^\intercal G_K^{-\intercal}$ (Guermah et al., 2008, Theorem 4). Furthermore, an input sequence $\left[\mathbf{u}^\intercal[K-1], \mathbf{u}^\intercal[K-2], \dots \mathbf{u}^\intercal[0]\right]^\intercal$ that transfers $\mathbf{x}[0] \neq 0$ to $\mathbf{x}[K] = 0$ is given by

$$\begin{bmatrix} \mathbf{u}[K-1] \\ \mathbf{u}[K-2] \\ \vdots \\ \mathbf{u}[0] \end{bmatrix} = -[G_0 B G_1 B \dots G_{K-1} B]^\intercal G_K^{-\intercal} W_c^{-1}(0, K) \mathbf{x}[0]. \tag{24}$$

Similarly, a system is *observable* if and only if the initial state $\mathbf{x}[0]$ can be uniquely determined from the knowledge of the control input and observations. For continuous-time systems, the system is observable on an interval $[t_0, t_1]$ if $y(t) = Cx(t) = 0$ for $t \in [t_0, t_1]$ implies $x(t) = 0$ for $[t_0, t_1]$. Hence, the system in (6) is observable on $[t_0, t_1]$ if an only if the observability Gramian matrix $W = \int_{t_0}^{t_1} E_\alpha(A^\intercal(t - t_0)^\alpha) C^\intercal C E_\alpha(A(t - t_0)^\alpha)\, \mathrm{d}t$ is positive definite (Balachandran et al., 2013, Theorem 1).

For linear discrete-time fractional-order systems modeled by (11), the system is said to be observable if and only if there exists some $K > 0$ such that the initial state $\mathbf{x}[0]$ at time $k = 0$ can be uniquely determined from the knowledge of $\{\mathbf{u}[0], \dots, \mathbf{u}[K-1]\}$ and $\{\mathbf{y}[0], \dots, \mathbf{y}[K-1]\}$. Therefore, by Theorem 5 in Guermah et al. (2008), the linear discrete-time fractional-order system is observable if and only if there exists a finite time K such that $\mathrm{rank}(\mathcal{O}_K) = n$, where $\mathcal{O}_K = \left[CG_0, CG_1, \dots, CG_{K-1}\right]^\intercal$ or, equivalently, $\mathrm{rank}(W_o(0, K)) = n$, where $W_o(0, K) = \sum_{j=0}^{K-1} G_j^\intercal C^\intercal C G_j$. Furthermore, the initial state at $\mathbf{x}[0]$ is given by

$$\mathbf{x}[0] = W_o^{-1}(0, K) \mathcal{O}_K^\intercal [\tilde{\mathcal{Y}}_K - \mathcal{M}_K \tilde{\mathcal{U}}_K], \tag{25}$$

where $\tilde{\mathcal{U}}_K = \left[\mathbf{u}^\intercal[0], \mathbf{u}^\intercal[1], \dots, \mathbf{u}^\intercal[K-1]\right]$, $\tilde{\mathcal{Y}}_K = \left[\mathbf{y}^\intercal[0], \dots, \mathbf{y}^\intercal[K-1]\right]^\intercal$, and

$$\mathcal{M}_K = \begin{bmatrix} 0 & 0 & \dots & 0 & 0 \\ CG_0 B & 0 & \dots & 0 & 0 \\ CG_1 B & CG_0 B & \dots & 0 & 0 \\ CG_2 B & CG_1 B & \dots & 0 & 0 \\ \vdots & \vdots & \ddots & \vdots & \vdots \\ CG_{K-2} B & CG_{K-3} B & \dots & CG_0 B & 0 \end{bmatrix}.$$

6. Proportional–integral–derivative control

A *proportional–integral–derivative controller* (*PID controller* or *three-term controller*) is a control loop mechanism. It employs feedback and is commonly used in industrial control systems and a variety of other applications that need a continuously modulated control because of its simplicity and ease of implementation. A PID controller continuously computes an error value as the difference between the desired setpoint (SP) and a measured process variable (PV) and implements a correction based on proportional, integral, and derivative terms of the error (P, I, and D, respectively). For example, the proportional (P) term multiplies a given constant with the error, an integral (I) term sums the error in previous time steps, and the derivative (D) term examines the rate of change of the error. These components sum together to create the PID controller.

The interpretability and comprehensibility of PID controllers make them a typical choice across many applications and in many industries. It is possible, with the right set of parameters, that a PID controller can reach the desired setpoint in a controlled manner, with minimal delay and overshoot. For instance, it is well-known that in general the integral term decreases the steady-state error whereas the derivative term decreases the oscillations (Bennett, 2001; Shah & Agashe, 2016).

The work in Podlubny (1999) provides the framework for continuous-time fractional-order PID control, which we summarize next. The fractional order version of PID controllers is defined using the following transfer function

$$C(s) = k_p + \frac{k_i}{s^\lambda} + k_d s^\mu. \tag{26}$$

For $\lambda = 1$ and $\mu = 1$, we obtain the standard integer-order setting with three degrees of freedom: k_p, k_i, and k_d. However, in (26), we have five parameters to determine, yielding five independent specifications that we are forced to meet. If we place the controller in front of a plant, specified as $G(s)$, in a unity feedback loop, then the first specification is on the phase margin as it is tightly coupled with the stability of the control system. The equations that define the phase margin are $20 \log \left| C\left(w_{gc}\right) G\left(g_{gc}\right) \right| = 0$ dB and $\arg\left(C\left(w_{gc}\right) G\left(w_{gc}\right)\right) = -\pi + \varphi_{pm}$, where w_{gc} is the gain crossover frequency and φ_{pm} the phase margin.

Subsequently, we may force a flat magnitude response $|G(jw)C(jw)|$ around the gain crossover frequency. We can ensure this response, see Monje, Vinagre, Feliu, and Chen (2008), by setting the derivative $\frac{\mathrm{d}}{\mathrm{d}w}(\arg(C(jw)G(jw)))$ to zero when $w = w_{gc}$. Moreover, ensuring this constraint makes the closed-loop control system robust against variations in the gain of $G(s)$.

Another specification supposes that a controller introduces the property of noise rejection in high frequencies. This property can be accomplished by fixing a critical frequency, w_h. If this frequency is exceeded, then the magnitude of the transfer function $T = CG/(1 + CG)$ (corresponding to the complementary sensitivity function) will be smaller than a pre-selected level.

Next, we want to ensure that a good output disturbance is not rejected. To address this, we can force an upper bound (M) on the

sensitivity function's magnitude below a pre-defined frequency (w_s). Hence, it follows that

$$20\log|S(jw)|_{w\le w_s} = 20\log\left|\frac{1}{1+C(jw)G(jw)}\right|_{w\le w_s} \le M \text{ dB}.$$

In the final step, to achieve a zero steady-state error, we need to design the controller $C(s)$ with an integral component.

Notice that, although solving the necessary set of equations from the constraints above is one way to establish the parameters k_p, k_i, k_d, λ, and μ, this requires the prior knowledge of the model order, dead time, poles and zeros. In the scenario where we do not have this prior knowledge, we may resort to *autotuning* (Chen, Moore, Vinagre, & Podlubny, 2004; Monje et al., 2008).

Other frequency domain approaches based on unity-feedback that use fractional-order differ-integration have been studied in Oustaloup, Melchior, Lanusse, Cois, and Dancla (2000), Oustaloup et al. (2008). These techniques have been used in many applications, ranging from path planning for robotics (Melchior, Orsoni, Lavialle, & Oustaloup, 2001) to system identification (Malti & Victor, 2015). The following tutorials overview three generations of related controllers (Lanusse, Malti, & Melchior, 2013; Shah & Agashe, 2016). We outline the basics for the first generation controller, which is a constant-phase controller around the required open-loop gain crossover frequency ω_{gc} and is obtained through a band-limited real fractional differentiator

$$C(s) = C_0\left(\frac{1+s/\omega_l}{1+s/\omega_h}\right)^n,$$

where C_0, ω_l, ω_h, and $n \in \mathbb{R}$. This controller will ensure robustness of the phase margin when the plant phase is constant. However, to simultaneously take the control effort level and the steady-state error into account, the first-generation controller becomes

$$C_F(s) = C_0\left(\frac{\omega_I}{s}+1\right)^{n_I}\left(\frac{1+s/\omega_l}{1+s/\omega_n}\right)^n\frac{1}{(1+s/\omega_F)^{n_F}},$$

where $n_I, n_F \in \mathbb{N}$ and $\omega_I, \omega_F \in \mathbb{R}^+$. The robustness of the phase margin is guaranteed if ω_{gc} is within a frequency range for which the plant phase is constant (Lanusse et al., 2013).

7. Sliding mode control

In control systems, *sliding mode control* (SMC) is a nonlinear control method that adjusts the dynamics of a nonlinear system by applying a discontinuous control signal (a set-valued control signal). This control signal compels the system to "slide" along a cross-section of the system's normal behavior. In this case, the state-feedback control law is not a function continuous in time. Instead, it can switch between continuous structures based on the state space's current position to achieve the desired behavior. There are two stages in SMC: *(i)* the *reaching phase*, which is the phase that lasts until the hitting of a trajectory to the switching subspace; *(ii)* the *sliding mode*, which is the motion after the previous phase. A relevant property of stage *(ii)* is the robustness against disturbances and variations in the process parameters – i.e., the *invariance property*.

Now, we present a set of results regarding SMC for continuous-time fractional order systems. Given the nth order fractional dynamic system in (5) and the following switching function

$$\sigma(t) = \Lambda\left(x(t) - r(t)\right), \tag{27}$$

where $r(t)$ is a reference signal and Λ is a parameter designed to make the sliding manifold a stable subspace when $\sigma = 0$, where stability is defined in (20). This entails that, despite the process being nonlinear, the nominal plant model is linear. If $0 < \alpha < 1$ and r is the vector of differentiable command signals, then the goal of the reaching law approach is to get $\Delta^\alpha\sigma(t) = -k\,\mathrm{sgn}(\sigma(t))$ for some $k > 0$. When $\alpha = 1$, it corresponds to $\dot\sigma(t) = -k\,\mathrm{sgn}(\sigma(t))$, which ensures $\sigma(t)\dot\sigma(t) < 0$ whenever $\sigma \neq 0$. This solution is the time derivative of the Lyapunov function $V = \frac{1}{2}\sigma(t)^2$, where the physical meaning of the time derivative of the Lyapunov function is to provide the sliding manifold with an attractor such that, once the error vector gets trapped to it, then the subsequent motion takes place in the proximity of the sliding hypersurface.

Next, we need to show that the aforementioned mechanism also works for non-integer differentiation order (Vinagre & Calderón, 2006). We start by differentiating $\Delta^\alpha\sigma(t) = -k\,\mathrm{sgn}(\sigma(t))$ at the order $-\alpha$, so we obtain

$$\Delta^1\left(\Delta^{-\alpha}\left(\Delta^\alpha\sigma(t)\right)\right) = -k\Delta^1\left(\Delta^{-\alpha}\,\mathrm{sgn}(\sigma(t))\right).$$

Then, we differentiate at order unity to obtain $\dot\sigma(t)$ given as

$$\dot\sigma(t) = -k\Delta^{1-\alpha}\,\mathrm{sgn}(\sigma(t)).$$

Because $0 < \alpha < 1$, it follows that $\mathrm{sgn}\left(\Delta^{1-\alpha}\,\mathrm{sgn}(\sigma(t))\right) = \mathrm{sgn}(\sigma(t))$. Forcing $\Delta^\alpha\sigma(t) = -k\,\mathrm{sgn}(\sigma(t))$ makes the locus described by $\sigma = 0$ a global attractor.

It is easy to check that choosing $\Delta^\alpha\sigma(t) = -k\,\mathrm{sgn}(\sigma(t)) - p\sigma(t)$ with $p > 0$ has the same effect on the reaching dynamics of integer-order. Notice that with $p\sigma = p|\sigma(t)|\,\mathrm{sgn}(\sigma)$, the following relation holds between $\dot\sigma(t)$ and $\mathrm{sgn}(\sigma(t))$:

$$\begin{aligned}\dot\sigma(t) &= -k\Delta^{1-\alpha}\,\mathrm{sgn}(\sigma(t)) - p\Delta^{1-\alpha}(|\sigma(t)|\,\mathrm{sgn}(\sigma(t)))\\ &= -\Delta^{1-\alpha}((k+p|\sigma(t)|)\,\mathrm{sgn}(\sigma(t))).\end{aligned}$$

Notice that, since $\mathrm{sgn}\left(\Delta^{1-\alpha}\,\mathrm{sgn}(\sigma(t))\right) = \mathrm{sgn}(\sigma)$, the reaching dynamics, governed by the above expression, generate a stronger push from both sides of the switching manifold. This effect translates into a higher attraction strength of the switching manifold for any $\sigma(t)$ with $p \neq 0$ than it does for $p = 0$. Moreover, for a fixed $\sigma(t)$, larger values of p create larger values of $\dot\sigma(t)$, which leads to reaching the place characterized by $\sigma = 0$ more quickly. If we select the Lyapunov function $V(t) = \frac{1}{2}\sigma(t)^2$ and compute its αth order derivative, using the Leibniz's differentiation rule, we obtain

$$\Delta^\alpha V(t) = \sum_{k=0}^{\infty}\frac{\Gamma(1+\alpha)}{\Gamma(1+k)}\Gamma(1-k+\alpha)\Delta^k\sigma(t)\Delta^{\alpha-k}\sigma(t),$$

i.e., an expression with infinitely many terms. Therefore, we are not able to infer the attractiveness of $\sigma(t) = 0$, deduced from $\sigma(t)\Delta^\alpha\sigma(t) < 0$, or more specifically, from $\Delta^\alpha\sigma(t) = -k\,\mathrm{sgn}(\sigma(t)) - p\sigma(t)$.

Recalling definition (1), the following equality holds

$$\sigma(t)\Delta^\alpha\sigma(t) = \frac{\sigma(t)}{\Gamma(1-\alpha)}\int_0^t\frac{\Delta\sigma(\tau)}{(t-\tau)^\alpha}\mathrm{d}\tau.$$

The previous relation imposes two possibilities to have $\sigma(t)\Delta^\alpha\sigma(t) < 0$:

(i) if $\sigma(t) > 0$, then $\Delta\sigma(t)$ (the first derivative of $\sigma(t)$) must be negative;
(ii) if $\sigma(t) < 0$, then $\Delta\sigma(t)$ (the first derivative of $\sigma(t)$) must be positive.

In conclusion, an appropriately designed control law is sufficient for closed-loop stability, forcing $\sigma\Delta^\alpha\sigma(t) < 0$. Therefore, the stability requirement $\sigma(t)\dot\sigma(t) < 0$ (or $\sigma(t)\Delta\sigma(t) < 0$) of the integer-order system is obtained naturally, whenever we impose $\sigma(t)\Delta^\alpha\sigma(t) < 0$.

In Efe (2011), the following is proposed. Compute the αth-order derivative of (27), which is

$$\Delta^\alpha\sigma(t) = \mathbf{\Lambda}\left(\Delta^\alpha x(t) - \Delta^\alpha r(t)\right) = \mathbf{\Lambda}\left(\mathbf{f}(x(t)) + \mathbf{g}(x(t))u(t) - \Delta^\alpha r(t)\right).$$

Next, setting the previous expression equal to $-k\,\mathrm{sgn}(\sigma(t)) - p\sigma(t)$ and solving for u yields the following control signal

$$u(t) = \frac{-\Lambda\mathbf{f}(x(t)) + \Lambda\Delta^\alpha r(t) - k\,\mathrm{sgn}(\sigma(t)) - p\sigma(t)}{\Lambda g(x(t))}, \tag{28}$$

where $\Lambda g(x(t)) \neq 0$. Having the encountered control law, deduced from a nominal model, an important question is to determine what the response of the system would be whenever the model in (5) is a nominal representation of a plant with uncertainties $\Delta\mathbf{f}(x(t))$ and $\Delta\mathbf{g}(x(t))$, such as

$$\Delta^\alpha x(t) = (\mathbf{f}(x(t)) + \Delta\mathbf{f}(x(t))) + (\mathbf{g}(x(t)) + \Delta\mathbf{g}(x(t)))u(t). \tag{29}$$

Combining (28) and (29) yields the following dynamics

$$\begin{aligned}\Delta^{\alpha}\sigma(t) = &-\left(1+\frac{\boldsymbol{\Lambda}\Delta\mathbf{g}(x(t))}{\boldsymbol{\Lambda}\mathbf{g}(x(t))}\right)(k\,\mathrm{sgn}(\sigma(t))+p\sigma(t))\\ &+\frac{\boldsymbol{\Lambda}\Delta\mathbf{g}(x(t))}{\boldsymbol{\Lambda}\mathbf{g}(x(t))}\boldsymbol{\Lambda}\left(\Delta^{\alpha}r(t)-\mathbf{f}(x(t))\right)+\boldsymbol{\Lambda}\Delta\mathbf{f}(x(t)).\end{aligned} \tag{30}$$

Hence, we have the following properties:

- If there are no uncertainties, i.e., $\Delta\mathbf{f}(x(t)) = \Delta\mathbf{g}(x(t)) = 0$, then we have $\Delta^{\alpha}\sigma(t) = -k\,\mathrm{sgn}(\sigma(t)) - p\sigma(t)$ to observe the sliding regime after hitting the sliding hypersurface;
- If $\Delta\mathbf{g}(x(t)) = 0$ and the columns of $\Delta\mathbf{f}(x(t))$ are in the range space of $\mathbf{g}(x(t))$, then $\Delta^{\alpha}\sigma(t) = -k\,\mathrm{sgn}(\sigma(t)) - p\sigma + \boldsymbol{\Lambda}\Delta\mathbf{f}(x(t))$. This case requires that condition $|A\Delta\mathbf{f}(x(t))| < k$ hold to ensure that $\sigma(t)\Delta^{\alpha}\sigma(t) < 0$;
- If the uncertainty terms are nonzero, then (30) is valid, which implies that the designer has to carefully set k and p to keep the attractiveness of the subspace defined by $\sigma(t) = 0$ The following two conditions are required to ensure that $\sigma(t)\Delta^{\alpha}\sigma(t) < 0$:

$$\begin{aligned}\left|\frac{\Lambda\Delta g(x(t))}{\Lambda g(x(t))}\right| &< 1\\ \left(1+\frac{\Lambda\Delta g(x(t))}{\Lambda g(x(t))}\right)k &> \left|\frac{\Lambda\Delta g(x(t))}{\Lambda g(x(t))}\Lambda\left(\Delta^{\alpha}r(t)-f(x(t))\right)+\Lambda\Delta f(x(t))\right|.\end{aligned}$$

The columns of $\Delta\mathbf{f}(x(t))$ and $\Delta\mathbf{g}(x(t))$ are assumed to be in the range space of $\mathbf{g}(x(t))$, i.e., the uncertainties are matched. If the previous condition is not satisfied, then the closed-loop performance will deteriorate.

Finally, notice that the first hitting to the switching subspace occurs when $t = t_h$, where $t_h = (|\sigma(0)|\Gamma(\alpha+1)/k)^{1/\alpha}$.

8. Backstepping control

Backstepping is a technique developed in the 1990s by Petar V. Kokotovic and others (Kokotovic, 1992; Lozano et al., 1992). The goal of this technique is to design stabilizing controls for a special class of nonlinear dynamical systems. These systems consist of subsystems that radiate out from an irreducible subsystem, which we can stabilize using some method. Due to its recursive structure, the designer can start the design process at the known stable system and "back out" new controllers that progressively stabilize each outer subsystem. The process of stabilization stops when the final external control is achieved. In other words, backstepping is based on the definition of a set of intermediate variables and the process of ensuring the negativity of Lyapunov functions that are combined to form a common control Lyapunov function for the overall system.

In fact, we can use the backstepping technique in a particular but wide class of systems. Consider the following system

$$\begin{aligned}\Delta^{\alpha_1}x_1(t) &= x_2(t)\\ \Delta^{\alpha_2}x_2(t) &= \mathbf{f}\left(x_1(t),x_2(t)\right)+\mathbf{g}\left(x_1(t),x_2(t)\right)u(t),\end{aligned} \tag{31}$$

where x_1 and x_2 are the state variables, $0 < \alpha_1, \alpha_2 < 1$ are positive fractional differentiation orders, $\mathbf{f}$ and $\mathbf{g}$ are known and smooth functions of the state variables such that $\mathbf{g}(x_1(t), x_2(t)) \neq 0$. Additionally, consider the intermediate variables of backstepping design:

$$\begin{aligned}z_1(t) &= x_1(t) - r_1(t) - A_1(t)\\ z_2(t) &= x_2(t) - r_2(t) - A_2(t),\end{aligned}$$

where $A_1(t) = 0$, $A_2(t)$ is an intermediate variable of backstepping design, and $\Delta^{\alpha_1}r_1(t) = r_2(t)$.

Subsequently, consider the Lyapunov function with variable of interest z

$$V(t) = \frac{1}{2}z^2(t).$$

Now, from Section 7, we have that $z(t)\Delta^{\alpha}z(t)$ ensures $z(t)\dot{z}(t) < 0$, for any $0 < \alpha < 1$. That said, we formulate the backstepping control technique for the plant described by (31) by recurrently checking the quantities $z_1(t)\Delta^{\alpha_1}z_1(t)$ and $z_1(t)\Delta^{\alpha_1}z_1(t) + z_2(t)\Delta^{\alpha_2}z_2(t)$ as the following steps:

1. Check $z_1(t)\Delta^{\alpha_1}z_1(t)$:

$$\begin{aligned}z_1(t)\Delta^{\alpha_1}z_1(t) &= z_1(t)\left(\Delta^{\alpha_1}x_1(t) - \Delta^{\alpha_1}r_1(t)\right)\\ &= z_1(t)\left(x_2(t) - r_2(t)\right)\\ &= z_1(t)\left(z_2(t) + r_2(t) + A_2(t) - r_2(t)\right)\\ &= z_1(t)\left(z_2(t) + A_2(t)\right)\end{aligned}$$

2. Choose $A_2(t) = -k_1z_1(t)$, with $k_1 > 0$, this would entail that

$$z_1(t)\Delta^{\beta_1}z_1(t) = -k_1z_1^2(t) + z_1(t)z_2(t)$$

3. Check $z_1(t)\Delta^{\alpha_1}z_1(t) + z_2(t)\Delta^{\alpha_2}z_2(t)$:

$$\begin{aligned}&z_1(t)\Delta^{\alpha_1}z_1(t) + z_2(t)\Delta^{\alpha_2}z_2(t)\\ &= -k_1z_1^2(t) + z_1(t)z_2(t) + z_2(t)\left(\Delta^{\alpha_2}x_2(t) - \Delta^{\alpha_2}r_2(t) - \Delta^{\alpha_2}A_2(t)\right)\\ &= -k_1z_1^2(t) + z_2(t)\left(\Delta^{\alpha_2}x_2(t) - \Delta^{\alpha_2}r_2(t) - \Delta^{\alpha_2}A_2(t) + z_1(t)\right)\\ &= -k_1z_1^2(t) + z_2(t)\Big(\mathbf{f}\left(x_1(t),x_2(t)\right) + \mathbf{g}\left(x_1(t),x_2(t)\right)u(t)\\ &\qquad - \Delta^{\alpha_2}r_2(t) - \Delta^{\alpha_2}A_2(t) + z_1(t)\Big)\end{aligned}$$

4. Force $z_1(t)\Delta^{\alpha_1}z_1(t) + z_2(t)\Delta^{\alpha_2}z_2(t) = -k_1z_1^2(t) - k_2z_2^2(t)$, with $k_2 > 0$, which implies that

$$\mathbf{f}(x_1(t),x_2(t)) + \mathbf{g}(x_1(t),x_2(t))u(t) - \Delta^{\alpha_2}r_2(t) - \Delta^{\alpha_2}A_2(t) + z_1(t) = -k_2z_2(t)$$

5. Obtain for u:

$$u(t) = -\frac{\mathbf{f}\left(x_1(t),x_2(t)\right) - \Delta^{\alpha_2}r_2(t) + k_1(t)\Delta^{\alpha_2}z_1(t) + z_1(t) + k_2z_2(t)}{\mathbf{g}\left(x_1(t),x_2(t)\right)}.$$

In fact, we can generalize the aforementioned procedure for systems of higher order of the form

$$\begin{aligned}\Delta^{\alpha_i}x_i(t) &= x_{i+1}(t), \quad \text{for } i = 1,\dots,q-1\\ \Delta^{\alpha_q}x_q(t) &= \mathbf{f}\left(x_1(t),\dots,x_q(t)\right)+\mathbf{g}\left(x_1(t),\dots,x_q(t)\right)u(t),\end{aligned}$$

where the resulting control law, in this case, is

$$u(t) = -\frac{\mathbf{f}(x_1(t),\dots,x_q(t)) - \Delta^{\alpha_q}r_q(t) - \Delta^{\alpha_q}A_q(t) + z_{q-1}(t) + k_qz_q(t)}{\mathbf{g}(x_1(t),\dots,x_q(t))}, \tag{32}$$

where $k_j > 0$, for $j = 1,\dots,q$, and A_i is given by the following recurrence relation:

$$\begin{aligned}&A_1(t) = 0, \qquad z_0(t) = 0\\ &A_{i+1}(t) = -k_iz_i(t) + \Delta^{\alpha_i}A_i(t) - z_{i-1}(t), \quad \text{for } i = 1,\dots,q-1.\end{aligned}$$

Now, the result of applying the control law in detailed in (32) is

$$\sum_{i=1}^{q} z_i(t)\Delta^{\alpha_i}z_i(t) = -\sum_{i=1}^{q} k_iz_i^2(t). \tag{33}$$

Finally, to ensure the negativeness of the right-hand side of (33) is the same as to ensure the negativity of $\sum_{i=1}^{q} z_i(t)\dot{z}_i(t)$, and the trajectories in the coordinate system spanned by $z_1(t),\dots,z_q(t)$ will converge the origin point.

9. Adaptive control

Adaptive control is the control method used by a controller that must adapt to a system with parameters that either vary over time or are initially uncertain. Therefore, it is desirable to have a control law that adapts itself to the changing conditions. In other words, adaptive control is a good alternative for industrial applications where the process parameters change, and the controller needs to automatically adapt itself to the new operating conditions. This aptitude is called adaptiveness. Here, the role of fractional calculus is to design non-integer-order adaptation laws or select reference models of non-integer-order (Monje et al., 2010).

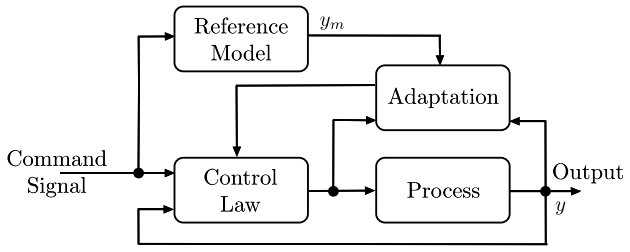

Fig. 1. Diagram of the MRAC control scheme.

A broadly adopted adaptive control structure is the so-called *model reference adaptive control* (MRAC) – see Fig. 1. This control strategy is grounded on the assumption that the changes in the process parameters are slower than other changes in the closed-loop system. Hence, the parameter adjustment mechanism employs the difference between the model output ($y_m(t)$) and the process response ($y(t)$) and uses the gradient rule to adjust the parameters of the control law:

$$\Delta^{\alpha}\phi(t) = -\eta\frac{\partial J(t)}{\partial \phi(t)} = -\eta e(t)\frac{\partial e(t)}{\partial \phi(t)}, \tag{34}$$

where $\phi(t)$ is a generic parameter of the control law, $e(t) = y(t) - y_m(t)$ is the instantaneous model following error, and $J(t) = \frac{e^2(t)}{2}$ is the instantaneous performance measure.

It is worth noticing that, when $\alpha = 1$ as in (34), we get the traditional linear-time invariant update laws. Additionally, we refer to Monje et al. (2010) for a detailed example considering a fractional-order reference model, where stability is also sought. Furthermore, the benefit of using a fractional-order system in MRAC is that it is possible to achieve a shorter transient regime compared to the classical case for linear time-invariant systems. This property might be critical in applications demanding a high-speed response.

10. System identification

Learning a fractional-order dynamical system's parameters, i.e., the fractional-order coefficients and the spatiotemporal matrix, is challenging. Specifically, the maximum-likelihood approach poses limitations due to the nonlinearity of the objective. However, some approaches were successfully developed for discrete-time linear fractional-order systems in Gupta et al. (2018a, 2018b, 2019), where an approximate solution is based on a variant of the expectation–maximization algorithm. Nonetheless, such approaches do not enable a finite-time assessment of the uncertainty associated with the parameters, which play a key role in the context of CNS.

Therefore, in what follows, we present a recent approach that relies on a bilevel iterative bisection scheme (Chatterjee & Pequito, 2022) to perform identification of the spatial and temporal parameters of a linear discrete-time fractional-order system. First, consider

$$\tilde{x}[k] = \begin{bmatrix} x[k] \\ x[k-1] \\ \vdots \\ x[k-p+1] \end{bmatrix} \tag{35}$$

as the *augmented* state vector and assuming that the system is *causal*, i.e., the state and disturbances are all considered to be zero before the initial time (i.e., $x[k] = 0$ and $w[k] = 0$ for all $k < 0$), we have

$$\begin{aligned}\tilde{x}[k+1] &= \underbrace{\begin{bmatrix} A_0 & \dots & A_{p-2} & A_{p-1} \\ I & \dots & 0 & 0 \\ \vdots & \ddots & \vdots & \vdots \\ 0 & \dots & I & 0 \end{bmatrix}}_{\tilde{A}}\tilde{x}[k] + \underbrace{\begin{bmatrix} I \\ 0 \\ \vdots \\ 0 \end{bmatrix}}_{\tilde{B}^w} w[k] \\ &= \tilde{A}\tilde{x}[k] + \tilde{B}^w w[k],\end{aligned} \tag{36}$$

for all $k \geq 0$. Note that (36) is an LTI system model, which we refer to as the *p-augmented LTI approximation* of (11).

Having established the p-augmented LTI approximation of a DTLFOS in (36), we can consider the two-level iterative bisection-like approach to identify the spatial and temporal parameters of the DTLFOS in (11). In particular, we start by noting the fact that for the Grünwald–Letnikov definition of the fractional derivative provided in (12), $\alpha_i = 1$ and $\alpha_i = -1$ can be interpreted, respectively, to be the discretized version of the derivative and the integral for $1 \leq i \leq n$, as defined in the sense of ordinary calculus.

To proceed with a bisection-like approach to identify $\{\alpha_i\}_{i=1}^n$ and $\tilde{A}$, we first fix the endpoints of the search space for α_i to be $\underline{\alpha_i} = -1$ and $\overline{\alpha_i} = 1$ for $1 \leq i \leq n$. We also calculate the value of $\alpha_{c,i} = (\underline{\alpha_i} + \overline{\alpha_i})/2$. Now, given the values of $\underline{\alpha_i}$, $\overline{\alpha_i}$, and $\alpha_{c,i}$, we calculate, using the ordinary least squares (OLS) technique described in detail below, the row vectors $\underline{\tilde{a}_i}$, $\overline{\tilde{a}_i}$, and $\tilde{a}_{c,i}$, respectively, that guide the evolution of the states in the p-augmented LTI approximation

$$\tilde{x}_i[k+1] = \tilde{a}_i\tilde{x}_i[k] + \tilde{b}_i^w w_i[k], \tag{37}$$

where $\tilde{a}_i = \underline{\tilde{a}_i}$ when $\alpha_i = \underline{\alpha_i}$, $\tilde{a}_i = \overline{\tilde{a}_i}$ when $\alpha_i = \overline{\alpha_i}$, and $\tilde{a}_i = \tilde{a}_{c,i}$ when $\alpha_i = \alpha_{c,i}$ with $\tilde{b}_i^w$ being obtained by extracting the ith row of $\tilde{B}^w$ for $1 \leq i \leq n$.

Next, we propagate the dynamics according to the obtained values of the parameters $\tilde{a}_i$ and calculate the mean squared error (MSE) between the states obtained as a result of the estimated $\tilde{a}_i$'s and the observed states. If the MSE is smaller corresponding to the $\underline{\alpha_i}$ case, then we set $\overline{\alpha_i} = \alpha_{c,i}$. If the MSE is smaller corresponding to the $\overline{\alpha_i}$ case, then we set $\underline{\alpha_i} = \alpha_{c,i}$. This approach is repeated until $|\overline{\alpha_i} - \underline{\alpha_i}|$ does not exceed a certain pre-specified tolerance ε. Algorithm 1 summarizes the procedure of determining the spatial and temporal components of a DTLFOS using the two-level iterative bisection-like approach that we have outlined above.

Therefore, for the estimation of the temporal components of a DTLFOS, we specify the iteration complexity of the bisection-like process and then, we investigate the finite-sample complexity of computing the spatial parameters using a least squares approach.

First, numerical and experimental evidence suggests that the computation of the temporal parameters of a DTLFOS, using, e.g., a wavelet-like technique described in Flandrin (1992), does not directly depend on the number of samples or observations used for the aforementioned estimation procedure. Empirical evidence suggests that a small number of samples (usually 30 to 100) suffice in order to compute $\{\alpha_i\}_{i=1}^n$. Furthermore, we can certify the iteration complexity of the bisection method to find the spatial and temporal parameters of a DTLFOS. Specifically, the bisection-based technique detailed above to find the temporal components of a DTLFOS is minmax optimal and the number ν of iterations needed in order to achieve a certain specified tolerance ε when this technique is used is bounded above by

$$\nu \leq \left\lceil \log_2\left(\frac{2}{\varepsilon}\right)\right\rceil. \tag{38}$$

Secondly, we can now delve into the problem of identifying the spatial parameters using a least squares-like approach and its finite-time guarantees. We start with the p-augmented LTI model of (36), i.e.,

$$\tilde{x}[k+1] = \tilde{A}\tilde{x}[k] + \tilde{B}^w w[k]. \tag{39}$$

The OLS method then outputs the matrix $\underline{\tilde{A}}[K]$ as the solution of the following optimization problem

$$\underline{\tilde{A}}[K] := \underset{\tilde{A}\in\mathbb{R}^{d\times d}}{\operatorname{argmin}} \sum_{k=1}^{K} \frac{1}{2}\left\|\tilde{x}[k+1] - \tilde{A}\tilde{x}[k]\right\|_2^2, \tag{40}$$

by observing the state trajectory of (36), i.e., $\{x[0], x[1], \dots, x[K+1]\}$, and the process noise $w[k]$ being independent and identically distributed (i.i.d.) zero-mean Gaussian.

Algorithm 1 Learning the parameters of a DTLFOS

for $i = 1$ to n **do**
  Initialize $\underline{\alpha_i} = -1$, $\overline{\alpha_i} = 1$, and tolerance ϵ.
  Calculate $\alpha_{c,i} = (\underline{\alpha_i} + \overline{\alpha_i})/2$.
  Given the above values of $\underline{\alpha_i}$, $\overline{\alpha_i}$, and $\alpha_{c,i}$, find, using the ordinary least squares (OLS) method, the row vectors $\tilde{a}_i$, $\overline{\tilde{a}_i}$, and $\tilde{a}_{c,i}$, respectively, that guide the evolution of the states in the p-augmented LTI approximation $\tilde{x}_i[k+1] = \tilde{a}_i \tilde{x}_i[k] + \tilde{b}_i^w w_i[k]$.
  Propagate the dynamics according to the obtained OLS estimates and calculate the mean squared error (MSE) between the propagated states and the observed state trajectory.
  if MSE is lower for the $\underline{\alpha_i}$ case **then**
    Set $\overline{\alpha_i} = \alpha_{c,i}$.
  else if MSE is lower for the $\overline{\alpha_i}$ case **then**
    Set $\underline{\alpha_i} = \alpha_{c,i}$.
  end if
  Terminate if $|\overline{\alpha_i} - \underline{\alpha_i}| < \epsilon$, else return to step 3.
end for

Thus, prior to characterizing the sample complexity of the OLS method for the p-augmented LTI approximation of the DTLFOS, we define a few quantities of interest. The *finite-time controllability Gramian* of the approximated system (36), W_t, is defined by

$$W_t := \sum_{j=0}^{t-1} \tilde{A}^j (\tilde{A}^j)^\mathsf{T}. \tag{41}$$

Intuitively, the controllability Gramian gives a quantitative measure of how much the system is excited when induced by the process noise $w[k]$ acting as an input to the system.

Additionally, given a symmetric matrix $A \in \mathbb{R}^{d\times d}$, we define $\lambda_{\max}(A)$ and $\lambda_{\min}(A)$ to denote, respectively, the maximum and minimum eigenvalues of the matrix A.

Lastly, for any square matrix $A \in \mathbb{R}^{d\times d}$, the *spectral radius* of the matrix A, $\rho(A)$, is given by the largest absolute value of its eigenvalues. Also, the *operator norm* of a matrix is denoted by

$$\|A\|_{\text{op}} = \inf\{c \geq 0 : \|Av\| \leq c\|v\| \text{ for all } v \in V\}.$$

Hence, we have the following result that characterizes the sample complexity of the above OLS method for the DTLFOS approximation. Fix $\delta \in (0, 1/2)$ and consider the p-augmented system in (36), where $\tilde{A} \in \mathbb{R}^{d\times d}$ is a marginally stable matrix (i.e., $\rho(\tilde{A}) \leq 1$) and $w[k] \sim \mathcal{N}(0, \sigma^2 I)$. Then, there exist universal constants $c, C > 0$ such that,

$$\mathbb{P}\left[\left\|\underline{\tilde{A}}[K] - \tilde{A}\right\|_{\text{op}} \leq \frac{C}{\sqrt{K\lambda_{\min}(W_k)}} \times \sqrt{d\log\left(\frac{d}{\delta}\right) + \log\det\left(W_K W_k^{-1}\right)}\right] \geq 1 - \delta, \tag{42}$$

for any k, such that

$$\frac{K}{k} \geq c\left(d\log\left(\frac{d}{\delta}\right) + \log\det\left(W_K W_k^{-1}\right)\right) \tag{43}$$

holds.

Remark 1. We note here that although the operator norm parameter estimation error in (42) is stated in terms of $\tilde{A}$, the operator norm errors, associated with the matrices $A_0, A_1, \ldots, A_{p-1}$, are strictly lower compared to $\left\|\underline{\tilde{A}}[K] - \tilde{A}\right\|_{\text{op}}$, since $A_0, A_1, \ldots, A_{p-1}$ are submatrices of $\tilde{A}$, and for any operator norm, the operator norm of a submatrix is upper bounded by one of the whole matrices (see Lemma A.9 of Foucart and Rauhut (2013) for a proof).

Additionally, it is worth mentioning that a similar finite-sample complexity bound similar to the one presented before can also be derived when we consider the ordinary least squares identification of the spatial parameters of a DTLFOS with inputs. For instance, within the purview of epileptic seizure mitigation using intracranial EEG data, the objective is to suppress the overall length or duration of an epileptic seizure. Thus, the goal is to steer the state of the neurophysiological system in consideration away from seizure-like activity, using a control strategy like model predictive control (Chatterjee et al., 2020).

11. Minimum-energy state estimation

Most of the estimators that exist for fractional-order dynamical systems are obtained under the assumption that the disturbance and noise have Gaussian distributions (Miljković et al., 2017; Najar et al., 2009; Sabatier et al., 2012; Safarinejadian et al., 2016, 2018; Sierociuk & Dzieliński, 2006). However, such an assumption is not realistic in the context of neural systems as disturbance frequencies can only lie within a specific frequency band. Therefore, in what follows, we present the so-called *minimum-energy state estimation*, where it is assumed that the disturbance and noise are unknown, but deterministic and bounded uncertainties.

Now, consider a left-bounded sequence $\{x[k]\}_{k\in\mathbb{Z}}$ over k, i.e., with $\limsup_{k\to-\infty} \|x[k]\| < \infty$. Then, the Grünwald–Letnikov fractional-order difference, for any $\alpha \in \mathbb{R}^+$, can be re-written as

$$\Delta^\alpha x[k] := \sum_{j=0}^{\infty} c_j^\alpha x[k-j], \quad c_j^\alpha = (-1)^j \binom{\alpha}{j},$$
$$\binom{\alpha}{j} = \begin{cases} 1 & \text{if } j = 0, \\ \prod_{i=0}^{j-1} \frac{\alpha - i}{i+1} = \frac{\Gamma(\alpha+1)}{\Gamma(j+1)\Gamma(\alpha-j+1)} & \text{if } j > 0, \end{cases} \tag{44}$$

for all $j \in \mathbb{N}$. The summation in (44) is well-defined from the uniform boundedness of the sequence $\{x[k]\}_{k\in\mathbb{Z}}$ and the fact that $|c_j^\alpha| \leq \frac{\alpha^j}{j!}$, which implies that the sequence $\{c_j^\alpha\}_{j\in\mathbb{N}}$ is absolutely summable for any $\alpha \in \mathbb{R}^+$ (Alessandretti, Pequito, Pappas, & Aguiar, 2020; Sopasakis & Sarimveis, 2017).

With the above ingredients, a discrete-time fractional-order dynamical network with additive disturbance can be described, respectively, by the state evolution and output equations

$$\sum_{i=1}^{l} A_i \Delta^{a_i} x[k+1] = \sum_{i=1}^{r} B_i \Delta^{b_i} u[k] + \sum_{i=1}^{s} G_i \Delta^{g_i} w[k], \tag{45a}$$

$$z[k] = C_k' x[k] + v'[k], \tag{45b}$$

with the variables $x[k] \in \mathbb{R}^n$, $u[k] \in \mathbb{R}^m$, and $w[k] \in \mathbb{R}^p$ denoting the state, input, and disturbance vectors at time step $k \in \mathbb{N}$, respectively. The scalars $a_i \in \mathbb{R}^+$ with $1 \leq i \leq l$, $b_i \in \mathbb{R}^+$ with $1 \leq i \leq r$, and $g_i \in \mathbb{R}^+$ with $1 \leq i \leq s$ are the fractional-order coefficients corresponding, respectively, to the state, the input, and the disturbance. The vectors $z[k], v'[k] \in \mathbb{R}^q$ denote, respectively, the output and measurement disturbance at time step $k \in \mathbb{N}$. We assume that the (unknown but deterministic) disturbance vectors are bounded as

$$\|w[k]\| \leq b_w, \|v'[k]\| \leq b_{v'}, \ k \in \mathbb{N}, \tag{46}$$

for some scalars $b_w, b_{v'} \in \mathbb{R}^+$. We also assume that the control input $u[k]$ is known for all time steps $k \in \mathbb{N}$. We denote by $x[0] = x(0)$ the initial condition of the state at time $k = 0$. In the computation of the fractional-order difference, we assume that the system is *causal*, i.e., the state, input, and disturbances are all considered to be zero before the initial time (i.e., $x[k] = 0, u[k] = 0$, and $w[k] = 0$ for all $k < 0$).

Next, consider the quadratic weighted least-squares objective function

$$\mathcal{J}\left(x[0], \{w[i]\}_{i=0}^{N-1}, \{v'[j]\}_{j=1}^{N}\right) = \sum_{i=0}^{N-1} w[i]^\mathsf{T} Q_i^{-1} w[i] + \sum_{j=1}^{N} v'[j]^\mathsf{T} R_j^{-1} v'[j] + (x[0] - \hat{x}_0)^\mathsf{T} P_0^{-1} (x[0] - \hat{x}_0), \tag{47}$$

subject to the constraints

$$\sum_{i=1}^{l} A_i \Delta^{a_i} x[k+1] = \sum_{i=1}^{r} B_i \Delta^{b_i} u[k] + \sum_{i=1}^{s} G_i \Delta^{g_i} w[k] \tag{48a}$$

and

$$z[k] = C_k' x[k] + v'[k], \tag{48b}$$

for some $N \in \mathbb{N}$, with the weighting matrices Q_i $(0 \leq i \leq N-1)$, R_j $(1 \leq j \leq N)$, and P_0 chosen to be symmetric and positive definite, and $\hat{x}_0$ chosen to be the *a priori* estimate of the system's initial state. The minimum-energy estimation procedure seeks to solve the following optimization problem

$$\begin{aligned} &\underset{\{x[k]\}_{k=0}^{N},\{w[i]\}_{i=0}^{N-1},\{v'[j]\}_{j=1}^{N}}{\text{minimize}} && \mathcal{J}\left(x[0], \{w[i]\}_{i=0}^{N-1}, \{v'[j]\}_{j=1}^{N}\right) \\ &\text{subject to} && \text{(48a) and (48b)}, \end{aligned} \tag{49}$$

for some $N \in \mathbb{N}$.

To derive the solution to (49), we first start with some alternative formulations of the discrete-time fractional-order system in (45a) and (45b) and relevant definitions that will be used in the sequel. Then, we present the solution and some additional properties of the derived solution, i.e., the exponential input-to-state stability of the estimation error.

In what follows, we consider the mild technical assumption that $\sum_{i=1}^{l} A_i$ is invertible. Additionally, we consider a truncation of the last υ temporal components of (45a), which we will refer to as the υ-approximation for the DTLFOS. That being said, the DTLFOS model in (45a) can be equivalently written as

$$x[k+1] = \sum_{j=1}^{\infty} \breve{A}_j x[k-j+1] + \sum_{j=0}^{\infty} \breve{B}_j u[k-j] + \sum_{j=0}^{\infty} \breve{G}_j w[k-j], \tag{50}$$

where $\breve{A}_j = -\hat{A}_0^{-1}\hat{A}_j$, $\breve{B}_j = \hat{A}_0^{-1}\hat{B}_j$, and $\breve{G}_j = \hat{A}_0^{-1}\hat{G}_j$ with $\hat{A}_j = \sum_{i=1}^{l} A_i c_j^{a_i}$, $\hat{B}_j = \sum_{i=1}^{r} B_i c_j^{b_i}$, and $\hat{G}_j = \sum_{i=1}^{s} G_i c_j^{g_i}$. Furthermore, for any positive integer $\upsilon \in \mathbb{N}^+$, the DTLFOS model in (45a) can be recast as

$$\tilde{x}[k+1] = \tilde{A}_\upsilon \tilde{x}[k] + \tilde{B}_\upsilon u[k] + \tilde{G}_\upsilon r[k], \qquad \tilde{x}[0] = \tilde{x}_0, \tag{51a}$$

$$y[k+1] = C_{k+1}\tilde{x}[k+1] + v[k+1], \tag{51b}$$

where

$$r[k] = \sum_{j=\upsilon+1}^{\infty} \breve{A}_j x[k-j+1] + \sum_{j=\upsilon+1}^{\infty} \breve{B}_j u[k-j] + \sum_{j=0}^{\infty} \breve{G}_j w[k-j], \tag{52}$$

with the augmented state vector $\tilde{x}[k] = [x[k]^\mathsf{T}, \dots, x[k-\upsilon+1]^\mathsf{T}, u[k-1]^\mathsf{T}, \dots, u[k-\upsilon]^\mathsf{T}]^\mathsf{T} \in \mathbb{R}^{\upsilon\times(n+m)}$ and appropriate matrices $\tilde{A}_\upsilon$, $\tilde{B}_\upsilon$, and $\tilde{G}_\upsilon$, where $\tilde{x}_0 = [x_0^\mathsf{T}, 0, \dots, 0]^\mathsf{T}$ denotes the initial condition. The matrices $\tilde{A}_\upsilon$ and $\tilde{B}_\upsilon$ are formed using the terms $\{\breve{A}_j\}_{1\leq j\leq \upsilon}$ and $\{\breve{B}_j\}_{1\leq j\leq \upsilon}$, while the remaining terms $\{\breve{G}_j\}_{1\leq j<\infty}$ and the state and input components not included in $\tilde{x}[k]$ are absorbed into the term $\tilde{G}_\upsilon r[k]$. Furthermore, we refer to (51a) as the υ-*approximation* of the DTLFOS presented in (45a).

To obtain the minimum-energy estimator, let us consider the quadratic weighted least-squares objective function

$$\begin{aligned} \mathcal{J}\left(\tilde{x}[0], \{r[i]\}_{i=0}^{N-1}, \{v[j]\}_{j=1}^{N}\right) = &\sum_{i=0}^{N-1} r[i]^\mathsf{T} Q_i^{-1} r[i] + \sum_{j=1}^{N} v[j]^\mathsf{T} R_j^{-1} v[j] \\ &+ (\tilde{x}[0]-\hat{x}_0)^\mathsf{T} P_0^{-1} (\tilde{x}[0]-\hat{x}_0), \end{aligned} \tag{53}$$

subject to the constraints

$$\bar{x}[k+1] = \tilde{A}_\upsilon \bar{x}[k] + \tilde{B}_\upsilon u[k] + \tilde{G}_\upsilon \bar{r}[k], \tag{54a}$$

$$y[k+1] = C_{k+1}\bar{x}[k+1] + \bar{v}[k+1], \tag{54b}$$

for some $N \in \mathbb{N}$. The weighting matrices Q_i $(0 \leq i \leq N-1)$ and R_j $(1 \leq j \leq N)$ are chosen to be symmetric and positive definite. The term $\hat{x}_0$ denotes the *a priori* estimate of the (unknown) initial state of the system, with the matrix P_0 being symmetric and positive definite.

Subsequently, we consider the weighted least-squares optimization problem

$$\begin{aligned} &\underset{\{\bar{x}[k]\}_{k=0}^{N},\{\bar{r}[i]\}_{i=0}^{N-1},\{\bar{v}[j]\}_{j=1}^{N}}{\text{minimize}} && \mathcal{J}\left(\tilde{x}[0], \{r[i]\}_{i=0}^{N-1}, \{v[j]\}_{j=1}^{N}\right) \\ &\text{subject to} && \text{(54a) and (54a)}, \end{aligned} \tag{55}$$

for some $N \in \mathbb{N}$. We denote the state vector that corresponds to the solution of the optimization problem (55) by $\hat{x}[k]$. Then, $\hat{x}[k]$ satisfies the recursion

$$\hat{x}[k+1] = \tilde{A}_\upsilon \hat{x}[k] + \tilde{B}_\upsilon u[k] + K_{k+1}\left(y[k+1] - C_{k+1}\left(\tilde{A}_\upsilon \hat{x}[k] + \tilde{B}_\upsilon u[k]\right)\right), \tag{56}$$

given $0 \leq k \leq N-1$, with initial conditions specified for $\hat{x}_0$ and $\{u[j]\}_{j=0}^{k}$, and with the update equations

$$K_{k+1} = M_{k+1} C_{k+1}^\mathsf{T} (C_{k+1} M_{k+1} C_{k+1}^\mathsf{T} + R_{k+1})^{-1}, \tag{57a}$$

$$M_{k+1} = \tilde{A}_\upsilon P_k \tilde{A}_\upsilon^\mathsf{T} + \tilde{G}_\upsilon Q_k \tilde{G}_\upsilon^\mathsf{T}, \tag{57b}$$

and

$$\begin{aligned} P_{k+1} &= (I - K_{k+1}C_{k+1}) M_{k+1} (I - K_{k+1}C_{k+1})^\mathsf{T} + K_{k+1} R_{k+1} K_{k+1}^\mathsf{T} \\ &= (I - K_{k+1}C_{k+1}) M_{k+1}, \end{aligned} \tag{57c}$$

with symmetric and positive definite P_0.

Notice that the dynamics of the recursion in (56) (with the initial conditions on $\hat{x}_0$ and the values of $\{u[j]\}_{j=0}^{k}$ being known) along with the update Eqs. (57) together solve (55). It is interesting to note here that the output term $y[k+1]$ presented in (56) and (54a) is the output of the υ-approximated system (51), which, in turn, is simply a subset of the outputs $z[k+1]$ obtained from (45b), truncated υ time steps in the past, provided $v[k]$ and C_k are formed from the appropriate blocks of $v'[k]$ and C_k' for all $k \in \mathbb{N}$.

Secondly, the minimum-energy estimator has exponential input-to-state stability of the estimation error.

In order to prove the exponential input-to-state stability of the minimum-energy estimation error, we need to consider the following mild technical assumptions. Specifically, there exist constants $\underline{\alpha}, \overline{\alpha}, \beta, \gamma \in \mathbb{R}^+$ such that

$$\underline{\alpha} I \preceq \tilde{A}_\upsilon \tilde{A}_\upsilon^\mathsf{T} \preceq \overline{\alpha} I, \quad \tilde{G}_\upsilon \tilde{G}_\upsilon^\mathsf{T} \preceq \beta I, \text{ and } \quad C_k^\mathsf{T} C_k \preceq \gamma I, \tag{58}$$

for all $k \in \mathbb{N}$.

Additionally, notice that the *state transition matrix* for the dynamics in (51a) is given by

$$\Phi(k, k_0) = \tilde{A}_\upsilon^{(k-k_0)}, \quad \text{with} \quad \Phi(k_0, k_0) = I, \tag{59}$$

for all $k \geq k_0 \geq 0$. We also consider the *discrete-time controllability Gramian* associated with the dynamics (51a) described by

$$W_c(k, k_0) = \sum_{i=k_0}^{k-1} \Phi(k, i+1) \tilde{G}_\upsilon \tilde{G}_\upsilon^\mathsf{T} \Phi^\mathsf{T}(k, i+1), \tag{60}$$

and the *discrete-time observability Gramian* associated with (51a) to be

$$W_o(k, k_0) = \sum_{i=k_0+1}^{k} \Phi^\mathsf{T}(i, k_0) C_i^\mathsf{T} C_i \Phi(i, k_0), \tag{61}$$

for $k \geq k_0 \geq 0$. We also make the following assumptions regarding *complete uniform controllability* and *complete uniform observability* of the υ-approximated system in (51a).

As such, we have to also consider that the υ-approximated system (51a) is completely uniformly controllable, i.e., there exist constants $\delta \in \mathbb{R}^+$ and $N_c \in \mathbb{N}^+$ such that

$$W_c(k + N_c, k) \succeq \delta I, \tag{62}$$

for all $k \geq 0$. And, similarly, the υ-approximated system (51a) is completely uniformly observable, i.e., there exist constants $\varepsilon \in \mathbb{R}^+$ and $N_o \in \mathbb{N}^+$ such that

$$W_o(k+N_o,k) \succeq \varepsilon \boldsymbol{\Phi}^{\mathsf{T}}(k+N_o,k)\boldsymbol{\Phi}(k+N_o,k), \tag{63}$$

for all $k \geq 0$.

Next, we also present an assumption certifying lower and upper bounds on the weight matrices Q_k and R_{k+1} in (53). That is, without loss of generality, we assume that the weight matrices Q_k and R_{k+1} satisfy

$$\underline{\vartheta} I \preceq Q_k \preceq \overline{\vartheta} I \quad \text{and} \quad \underline{\rho} I \preceq R_{k+1} \preceq \overline{\rho} I, \tag{64}$$

for all $k \geq 0$ and constants $\underline{\vartheta}, \overline{\vartheta}, \underline{\rho}, \overline{\rho} \in \mathbb{R}^+$.

Hence, it is possible to establish lower and upper bounds for the matrix P_k but is not required to show that the estimation error is exponentially input-to-state stable. Specifically, the minimum-energy estimation error $e[k]$, given by

$$e[k] = \hat{x}[k] - \tilde{x}[k], \tag{65}$$

is such that there exist constants $\sigma, \tau, \chi, \psi \in \mathbb{R}^+$ with $\tau < 1$ such that the estimation error $e[k]$ satisfies

$$\|e[k]\| \leq \max\left\{ \sigma\tau^{k-k_0}\|e[k_0]\|,\ \chi \max_{k_o \leq i \leq k-1} \|r[i]\|,\ \psi \max_{k_o \leq j \leq k-1} \|v[j+1]\| \right\} \tag{66}$$

for all $k \geq k_0 \geq \max\{N_c, N_o\}$.

It is interesting to note that the bound on the estimation error $e[k]$ in (66) actually depends on $\|r[i]\|$, where $k_0 \leq i \leq k-1$ for all $i \in \mathbb{N}$. In fact, a distinguishing feature of DTLFOS is the presence of a finite non-zero disturbance term in the input-to-state stability bound of the tracking error when tracking a state other than the origin. This disturbance is dependent on the upper bounds on the non-zero reference state being tracked as well as the input. While the linearity of the Grünwald–Letnikov fractional-order difference operator allows one to mitigate this issue in the case of tracking a non-zero exogenous state by a suitable change of state and input coordinates, this approach is not one we can pursue in this paper, since the state we wish to estimate is unknown. However, it can be shown that as the value of υ in the υ-approximation increases, the upper bound associated with $\|r[i]\|$ decreases drastically since the υ-approximation gives us progressively better representations of the unapproximated system. This further implies that $\|r[i]\|$ in (66) stays bounded, with progressively smaller upper bounds associated with $\|r[i]\|$ (and hence, $\|e[k]\|$) with increasing υ.

Lastly, the estimation error associated with the minimum-energy estimation process in (65) is defined in terms of the state of the υ-approximated system $\tilde{x}[k]$. In reality, as detailed above, with larger values of υ, the υ-approximated system approaches the real system dynamics, and thus we obtain an expression for the estimation error with respect to the real system in the limiting case, where the input-to-state stability bound as presented in (66) holds.

12. Fractional optimal control

Fractional optimal control finds the optimal control strategy to manipulate a fractional-order dynamical system to achieve a specific goal. Usually the goal is to achieve a certain desired state behavior while minimizing the amount of control effort (Riewe, 1996). The fractional optimal control problem with a finite-time horizon can be formulated as follows:

$$\begin{aligned} &\text{(cost function)} && \underset{\mathbf{u}}{\text{minimize}} && \int_{t_0}^{T} (\mathbf{x}(t)-\mathbf{x}_d(t))^{\mathsf{T}} Q (\mathbf{x}(t)-\mathbf{x}_d(t)) + \mathbf{u}(t)^{\mathsf{T}} R \mathbf{u}(t)\ \mathrm{d}t \\ &\text{(constraints)} && \text{subject to} && \Delta^{\alpha}\mathbf{x}(t) = A\mathbf{x}(t) + B\mathbf{u}(t) \\ &&&&& \text{other linear constraints on } \mathbf{x}(t) \text{ and } \mathbf{u}(t), \end{aligned} \tag{67}$$

where $\mathbf{x}(t) \in \mathbb{R}^n$ is the state of the system, $\mathbf{x}_d(t) \in \mathbb{R}^n$ is the desired state of the system, $\mathbf{u}(t) \in \mathbb{R}^m$ is the control input, Q is the cost on the state achieving the desired behavior, R is the cost on the control effort, Δ^{α} is the Caputo fractional-order derivative, $A \in \mathbb{R}^{n\times n}$ is the state matrix, and $B \in \mathbb{R}^{n\times m}$ is the control input matrix.

Many mathematical techniques for solving fractional optimal control problems have been proposed, including numerical solvers (Agrawal, 2004; Agrawal & Baleanu, 2007; Baleanu, Defterli, & Agrawal, 2009; Nemati, Lima, & Torres, 2019) and discrete methods (Almeida & Torres, 2015). Other works have considered fractional optimal control using the following schemes, including distributed fractional optimal control (Zaky & Machado, 2017), a finite-time horizon (Biswas & Sen, 2011), multi-dimensional fractional optimal control (Agrawal, Defterli, & Baleanu, 2010), an Euler–Lagrange formulation (Agrawal, 2002; Frederico & Torres, 2007, 2008; Torres & Malinowska, 2012), and reinforcement learning (Gupta, Yin, Deshmukh, & Bogdan, 2021). Furthermore, fractional optimal control has been used in the following applications, including cloud computing (Ghorbani, Wang, Xue, Pedram, & Bogdan, 2014), regulating diabetes (Ghorbani & Bogdan, 2013, 2014), cyber–physical systems (Bogdan & Marculescu, 2011), regulating heart disease (Bogdan, Jain, Goyal & Marculescu, 2012; Bogdan, Jain, & Marculescu, 2013), data-centers-on-chip (Bogdan, 2015), power management (Bogdan, Marculescu, & Jain, 2013; Bogdan, Marculescu, Jain & Gavila, 2012), and chemical processing plants (Petráš, 2021).

Fractional optimal control is at the core of receding horizon approaches referred to as model predictive control, and overviewed in more detail next.

13. Model predictive control

Model predictive control (MPC) is a control strategy that allows the control of processes while satisfying a set of constraints. At its core, MPC uses explicit process models (which may be linear or nonlinear) to predict how a plant will respond to arbitrary inputs. For each instant of time, an MPC algorithm seeks to optimize plant behavior in the future by computing a series of control inputs over a time horizon called the *prediction horizon* by solving an optimization problem — often with constraints. Once this step is complete, the computed control inputs corresponding to the first subsection of the prediction horizon (called the *control horizon*) are then sent to the plant. This procedure is then repeated at subsequent control intervals (Qin & Badgwell, 2003). This receding horizon strategy implicitly introduces *closed-loop feedback*.

Next, we consider the case where the predictive model is a linear fractional-order system. Based on the state signal's evolution predicted by the model, and by regarding the impact of an arbitrary control input signal in the state's evolution, we can set out to adapt the stimulation signal in real-time by choosing the parameters that lead to stimulation signals within a safe range towards optimizing some measure of performance that encapsulates the goal of steering abnormal activity to normal ranges. In general, however, our predictive model will not precisely match the real dynamics of the system. Therefore, our proposed stimulation strategy will periodically re-evaluate the current estimated state and corresponding predictions and re-compute the appropriate optimal stimulation strategy.

First, in the fractional-order model predictive control framework, we will focus on the design of a model predictive controller for a (possibly time-varying) discrete-time fractional-order dynamical system model

$$\Delta^{\alpha} x[k+1] = A_k x[k] + B_k u[k] + B_k^{w} w[k], \tag{68}$$

where $w[k]$ denotes a sequence of independent and identically distributed random vectors, following an $\mathcal{N}(0,\Sigma)$ distribution (with the covariance matrix $\Sigma \in \mathbb{R}^{n\times n}$) and B_k^{w} denotes the matrix of weights that scales the noise term $w[k]$. The objective is to design the feedback controller such that it minimizes a quadratic cost functional of the input

and state vectors over a finite time horizon P (the prediction horizon). In other words, the objective is to determine the sequence of control inputs $u[k], \dots, u[k+P-1]$ that minimizes a quadratic cost function of the form

$$\begin{aligned}
&\text{(cost function)} \quad \underset{u[k],\dots,u[k+P-1]}{\text{minimize}} \quad \mathbb{E}\left\{ \sum_{j=1}^{P} \|x[k+j]\|^2_{Q_{k+j}} \right. \\
&\qquad + \sum_{j=1}^{P} c^{\mathsf{T}}_{k+j} x[k+j] \\
&\qquad \left. + \sum_{j=0}^{P-1} \|u[k+j]\|^2_{R_{k+j}} \right\} \\
&\text{(constraints)} \quad \text{subject to} \quad x[k] \\
&\qquad = \text{observed or estimated} \\
&\qquad \quad \text{current state} \\
&\qquad \Delta^{\alpha} x[k+j+1] \\
&\qquad = A_{k+j} x[k+j] + B_{k+j} u[k+j] \\
&\qquad + B^{w}_{k+j} w[k+j], \\
&\qquad j = 0, 1, \dots, P-1, \\
&\qquad \text{other linear constraints on} \\
&\qquad x[k+1], \dots, x[k+P], \\
&\qquad u[k], \dots, u[k+P-1],
\end{aligned} \tag{69}$$

where $Q_{k+1}, \dots, Q_{k+P} \in \mathbb{R}^{n \times n}$ and $R_k, \dots, R_{k+P-1} \in \mathbb{R}^{n_u \times n_u}$ are given positive semidefinite matrices. Here, $Q \in \mathbb{R}^{n \times n}$ is a *positive semidefinite* matrix if $x^{\mathsf{T}} Q x \geq 0$, for every $x \in \mathbb{R}^n$, and $\|x\|_Q = \sqrt{x^{\mathsf{T}} Q x}$ in that case.

The quadratic term on the input, which represents the electrical neurostimulation signal, is intended to add a penalization term for stimulating the patient too harshly, since this may be unsafe, create discomfort for the patient, or result in harmful psychological effects (Moratti & Patterson, 2014). It is also interesting to note that even if we need the estimation of the system states in the above problem, the presence of a separation principle for discrete-time fractional-order systems (Chatterjee, Romero, & Pequito, 2019) gives us guarantees that we can perform model predictive control with state estimation for these systems.

Note that, here, P is called the *prediction horizon*, and the framework only deploys the control strategy associated with the first M time steps (referred to as the *control horizon*). Simply speaking, after we reach state $x[k+M-1]$, we update k with $k+M-1$ and recompute the new solution. This way, we have robust solutions, since, by design, the optimal strategy is constantly being re-evaluated based on the short-term control action implementation of a long-term prediction (Bequette, 2013; Petráš, 2021).

14. Applications in cyber-neural systems

System identification

We present some preliminary results regarding the performance of the above approach. Specifically, we use 1000 noisy measurements taken from 4 channels of an intracranial electroencephalographic (iEEG) signal, which records the brain activity of subjects undergoing epileptic seizures. The signals were recorded and digitized at a sampling rate of 512 Hz at the Hospital of the University of Pennsylvania, Philadelphia, PA. Subdural grid and strip electrodes were placed at specialized locations (dictated by a multidisciplinary team of neurologists, neurosurgeons, and a radiologist), with the electrodes themselves consisting of linear and two-dimensional arrays spanning 2.3 mm in diameter and having a inter-contact spacing of 10 mm (Ashourvan et al., 2020; Khambhati et al., 2015).

The least squares optimization problems described in Section 10 are solved using the convex optimization package `CVX` (Grant & Boyd, 2008, 2014) in MATLAB with the aid of a window-based approach using a finite subset of the entire range of measurements. This is done because the time series under consideration is nonlinear, and it is not possible to characterize the entire gamut of measurements using very few parameters. Fig. 2 shows the performance of our method on the above data. Additionally, we also show in Fig. 3 the variation of the error of the least squares predictions with respect to the observed data, with varying window sizes in the least squares optimization problems. We see that the identified system parameters are able to predict the system states fairly closely, thus demonstrating that our approach can be used to learn the system parameters of a discrete-time fractional-order system.

Minimum-energy state estimation

In this section, we consider the performance of the minimum-energy estimation paradigm on real-world neurophysiological networks considering EEG data. Specifically, we use 150 noisy measurements taken from 4 channels of a 64-channel EEG signal which records the brain activity of subjects, as shown in Fig. 4. The subjects were asked to perform a variety of motor and imagery tasks. Furthermore, we select the 4 channels positioned over the motor cortex of the brain, which enables us to predict motor actions such as the movement of the hands and feet. The data was collected using the BCI2000 system with a sampling rate of 160 Hz (Goldberger et al., 2000; Schalk, McFarland, Hinterberger, Birbaumer, & Wolpaw, 2004). The spatial and temporal parameter components of the fractional-order system assumed to model the original EEG data were identified using the methods described in Gupta et al. (2018a). The matrices $B_i = \begin{bmatrix} 1 & 1 & 1 & 1 \end{bmatrix}^{\mathsf{T}}$ for all i.

The results of our approach, considering different values of $\mathfrak{v}$, are shown in Figs. 5 and 6 (for $\mathfrak{v} = 2$), Figs. 7 and 8 (for $\mathfrak{v} = 10$), and Figs. 9 and 10 (for $\mathfrak{v} = 20$), which show, respectively (for each value of $\mathfrak{v}$), the comparison between the measured output of the network with noise and the estimated response obtained from the minimum-energy estimator, and also the juxtaposition of the measurement error and the estimation error of the minimum-energy estimation process. We find that the minimum-energy estimator is successfully able to estimate the states in the presence of noise in both the dynamics and the measurement processes.

We also note from Figs. 5 and 6 that when $\mathfrak{v} = 2$, we get comparatively larger estimation errors associated with the last 50 or so samples of Channel 4 and that this behavior can be mitigated by increasing the value of $\mathfrak{v}$, e.g., by choosing $\mathfrak{v} = 10$ or $\mathfrak{v} = 20$. This is in line with the discussion at the end of Section 11, and choosing a larger value of $\mathfrak{v}$ can always, in practice, provide us with better estimation performances, as seen from this example.

Neurostimulation using fractional-order model predictive control for epileptic seizure mitigation

In what follows, we propose to illustrate the use of the fractional-order system model predictive control (FOS-MPC) framework for neurostimulation in the context of mitigating epileptic seizures. We demonstrate the workings of the proposed approach on four different experimental scenarios relying primarily on intracranial electroencephalographic (iEEG) data: *(i)* an iEEG signal demonstrating an epileptic seizure simulated by the neural mass model proposed by Jansen and Rit (Jansen & Rit, 1995; Jansen, Zouridakis, & Brandt, 1993); *(ii)* an iEEG signal simulated by a neural field model proposed by Martinet et al. in Martinet et al. (2017) that replicates the spatiotemporal dynamics of a seizure; *(iii)* an iEEG signal simulated by the phenomenological 'Epileptor' model proposed in Jirsa, Stacey, Quilichini, Ivanov, and Bernard (2014); and *(iv)* real-time iEEG signals for three human subjects undergoing epileptic seizures. For all of the above cases, we start by considering an epileptic seizure, captured by a linear fractional-order system (FOS) model, whose parameters are obtained through a system identification method using brainwave data obtained from iEEGs.

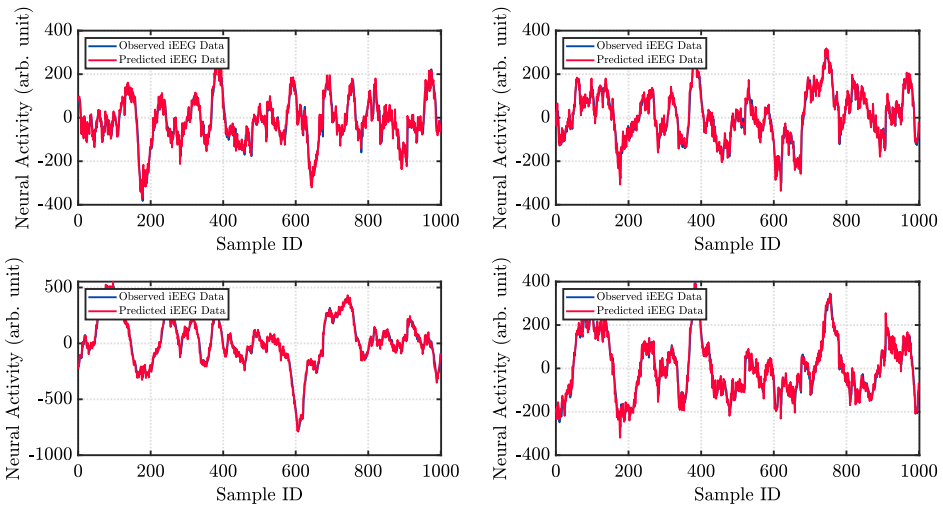

Fig. 2. Performance of our system identification approach on real-life intracranial EEG data. (For interpretation of the references to color in this figure legend, the reader is referred to the web version of this article.).

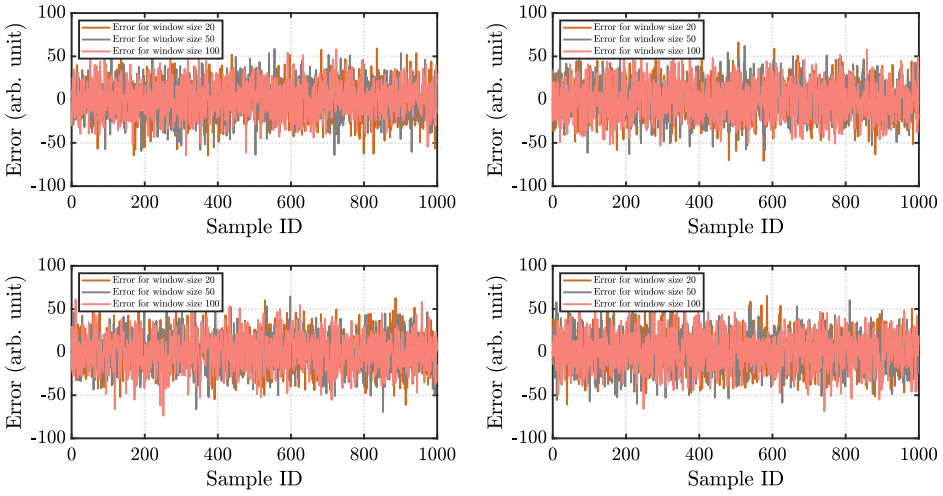

Fig. 3. Variation of the error of the least squares prediction with respect to the observed data, with varying window sizes in the least squares optimization problems. (For interpretation of the references to color in this figure legend, the reader is referred to the web version of this article.).

Epileptic seizure simulated by the jansen–rit neural mass model

Although initially proposed to account for human EEG rhythms and visual evoked potentials, the Jansen–Rit neural mass model (Jansen & Rit, 1995) has also been used to shed light on human epileptiform brain dynamics (Wendling, Bellanger, Bartolomei, & Chauvel, 2000; Wendling, Benquet, Bartolomei, & Jirsa, 2016). The Jansen–Rit neural mass model is composed of three interacting subpopulations that include: the main subpopulation, the excitatory feedback subpopulation, and the inhibitory feedback subpopulation. The structure of the model is such that the main subpopulation comprises cells that receive neuronal signals in feedback from the excitatory and inhibitory subpopulations.

The use of neural mass models akin to the Jansen–Rit model in feedback control frameworks is well documented. All the works in Soltan, Xia, Jackson, Chester, and Degenaar (2018), Wang, Niebur, Hu, and Li (2016), Wei, Wei, Xia, Zuo, and Shen (2019), Wei, Wei, and Zuo (2019), Wei, Wei, Zuo, Yu and Li (2019), Xia et al. (2019) use neural mass models, in the control theory sense, for the suppression of epileptic seizures. In what follows, we will demonstrate the effectiveness of our proposed control strategy on a seizure simulated by the classical Jansen–Rit neural mass model with standard parameter values.

First, we need to determine the parameters A and α that model both spatial coupling and fractional coefficients, respectively, that craft the evolution of the state $x[k] \in \mathbb{R}^n$ in the fractional-order system (FOS) model.

$$\Delta^{\alpha} x[k+1] = Ax[k] + Bu[k] + B^{w} w[k], \tag{70}$$

with $w[k]$ denoting additive white Gaussian noise (AWGN). Since the system is single-input-single-output (SISO), we have both A and α to be scalars. To identify the parameters A and α, we used the method proposed in Gupta et al. (2018a). The parameters obtained are $A = -0.0054$ and $\alpha = 1.4881$. Furthermore, we assume that $B = 1$ and $B^{w} = 0.1$.

For the cost function in (69), we utilized $Q_k = I_n$, $R_k = I_{n_u}$, and $c_k = 0_{n_u \times 1}$ (with $n = n_u = 1$), to emphasize minimizing the overall energy in the measured iEEG signal, while penalizing slightly for overly aggressive stimulation. Furthermore, we included a safety linear constraint of $-5 \leq u[k] \leq 5$. Our predictive model was based on a ($p = 15$)–step (15 ms) predictive model approximation of the FOS plant, with a ($P = 20$)–step (20 ms) prediction horizon and ($M = 10$)–step (10 ms) control horizon. The results are presented in Fig. 11, which provide evidence that the proposed stimulation strategy allows us to achieve amplitude suppression using a (time-varying) impulse-like stimulation scheme. Note that the actuation signal u_k kicks in at about the 4-second mark in the figure.

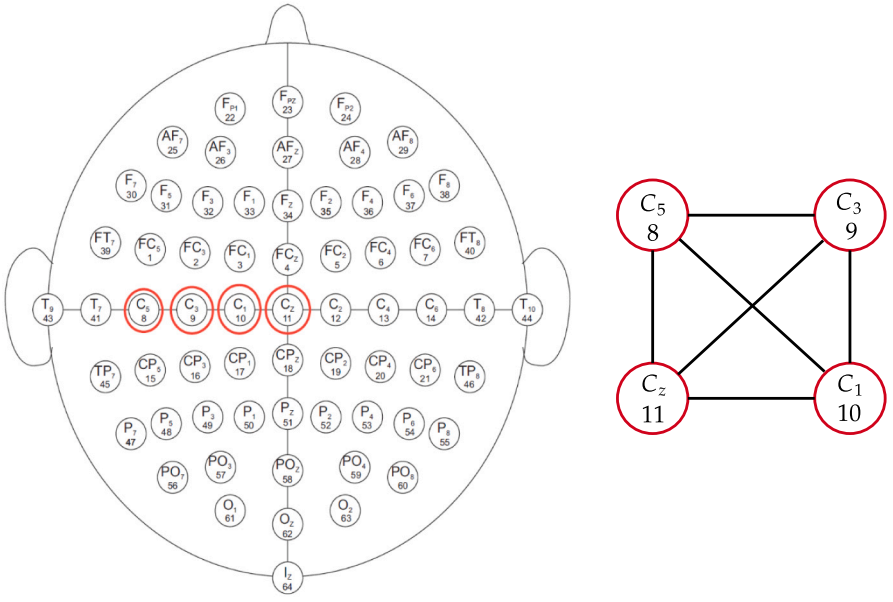

Fig. 4. The distribution of the sensors for the measurement of EEG data is shown on the left. The channel labels are shown along with their corresponding numbers and the selected channels over the motor cortex are shown in red. The corresponding network formed by the EEG sensors is shown on the right. (For interpretation of the references to color in this figure legend, the reader is referred to the web version of this article.).

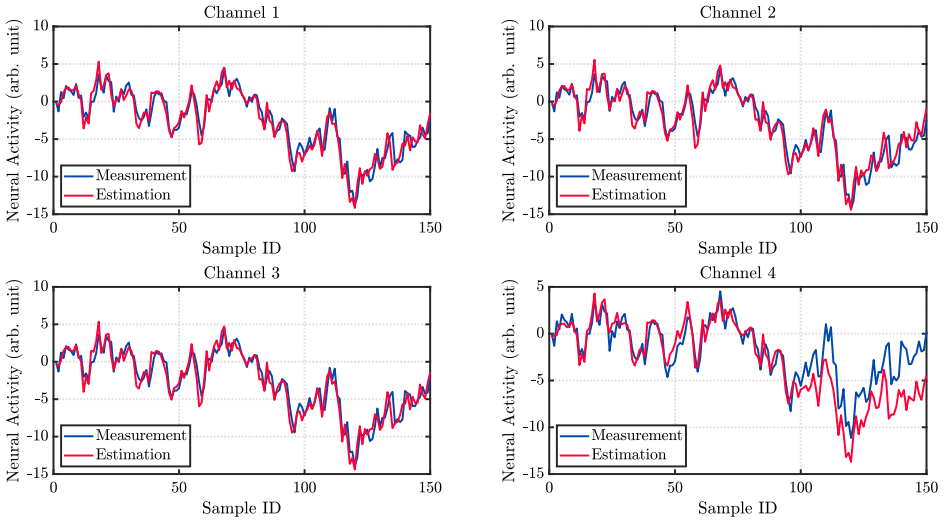

Fig. 5. Comparison between the measured output of the υ-augmented system (with $\upsilon = 2$) versus the estimated output of a minimum-energy estimator implemented on the same, in the presence of process and measurement noises for 4 channels of a 64-channel EEG signal. (For interpretation of the references to color in this figure legend, the reader is referred to the web version of this article.).

Epileptic seizure simulated by the mean-field model proposed by Martinet et al. (2017) .

Next, we turn our attention towards a computational model that uses traveling wave dynamics to capture inter-scale coupling phenomena between large-scale neural populations in the cortex and small-scale groups in cortical columns (Martinet et al., 2017). Modeling the complex spatiotemporal dynamics of epileptic seizures is a challenging task, mainly because of the interaction of myriad scales in both time and space.

The neural field model proposed by Martinet et al. in Martinet et al. (2017) is a modified version of the mean-field model proposed in Steyn-Ross, Steyn-Ross, and Sleigh (2013) that seeks to explain the phenomena, origin, and spatiotemporal dynamical properties of seizure propagation and spike-and-wave discharges (SWDs). Additionally, their work advances the hypothesis that increased diffusion of extracellular potassium concentrations in space influences the interlaced coupling of human seizures. In what follows, we will use the simulated seizure data obtained from the aforementioned model and then consider our closed-loop MPC neurostimulation scheme on the same model.

To determine the system parameters A and α in (70), we utilize roughly 2 seconds of pre-ictal activity captured by the model. Note that here, we will only consider $n = 4$ channels for our proposed approach to mimic the capabilities available in the NeuroPace® RNS® device. Applying the methods in Gupta et al. (2018a) yields the following FOS parameters:

$$A = \begin{bmatrix} 0.2969 & -0.0203 & -0.2922 & 0.0587 \\ 0.2574 & -0.1726 & -0.1905 & 0.1535 \\ 0.5348 & -0.1066 & -0.3471 & -0.0169 \\ 0.4007 & -0.6752 & 0.0044 & 0.3186 \end{bmatrix}, \tag{71}$$

and

$$\alpha = \begin{bmatrix} 0.8114 & 0.8334 & 0.8034 & 0.8413 \end{bmatrix}^{\mathsf{T}}. \tag{72}$$

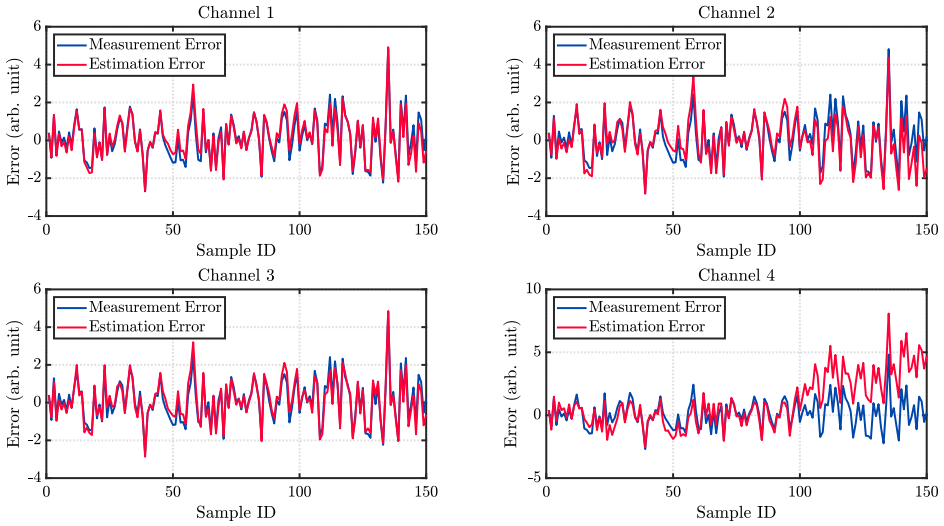

Fig. 6. Comparison between the measurement error of the υ-augmented system (with $\upsilon = 2$) versus the estimation error of a minimum-energy estimator implemented on the same, in the presence of process and measurement noises for 4 channels of a 64-channel EEG signal. (For interpretation of the references to color in this figure legend, the reader is referred to the web version of this article.).

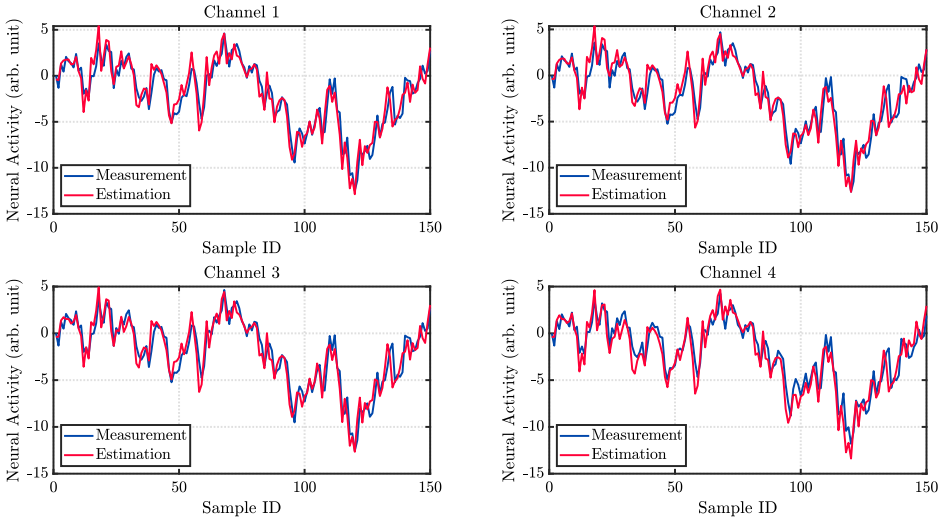

Fig. 7. Comparison between the measured output of the υ-augmented system (with $\upsilon = 10$) versus the estimated output of a minimum-energy estimator implemented on the same, in the presence of process and measurement noises for 4 channels of a 64-channel EEG signal. (For interpretation of the references to color in this figure legend, the reader is referred to the web version of this article.).

Additionally, we consider a single control signal u_k that affects all the channels equally, i.e., $B = \begin{bmatrix}1 & 1 & 1 & 1\end{bmatrix}^{\mathsf{T}}$ and the matrix of weights $B^w = 0.05 I_4$, with I_4 being the 4×4 identity matrix.

Using the FOS-MPC neurostimulation strategy with $Q_k = I_n$, $R_k = I_{n_u}$, and $c_k = 0_{n_u \times 1}$ (with $n = 4$ and $n_u = 1$), and safety linear constraints of $-100 \leq u[k] \leq 100$, we find from Fig. 12 that our proposed approach successfully suppresses seizure-like activity using a (time-varying) impulse-like stimulation scheme. In this case, we use a ($p = 10$)–step (20 ms) predictive model approximation of the FOS plant, with a ($P = 10$)–step (20 ms) prediction horizon, and ($M = 8$)–step (16 ms) control horizon. Here too, the actuation signal u_k kicks in at about the 4-second mark.

Epileptic seizure simulated by the epileptor, a phenomenological model of seizures by Jirsa et al. (2014)

Next, we investigate the performance of our proposed approach on the Epileptor model (Jirsa et al., 2014), which is a phenomenological model able to accurately reproduce the dynamics of a wide variety of human epileptic seizures recorded with iEEG electrodes.

The Epileptor model consists of a system of coupled nonlinear ordinary differential equations in five state variables and one dummy variable. The model can be thought of as two two-dimensional subsystems, one for generating fast discharges on a faster timescale and the other for generating sharp-wave events (SWEs) on an intermediate timescale. These two subsystems are linked and evolve on the very slow timescale of a permittivity variable. This allows for the autonomous transition between fast and slow pathological seizure states. The dynamics of the Epileptor can be represented as follows:

$$\begin{aligned}
\dot{x}_1 &= y_1 - f_1(x_1, y_1, z) - z + I_{\text{rest},1} \\
\dot{y}_1 &= y_0 - 5x_1^2 - y_1 \\
\tau_0 \dot{z} &= 4(x_1 - x_0) - z \\
\dot{x}_2 &= -y_2 + x_2 - x_2^3 + I_{\text{rest},2} + 2u - 0.3(z - 3.5) \\
\tau_2 \dot{y}_2 &= -y_2 + f_2(x_2) \\
\dot{u} &= -\gamma(u - 0.1x_1),
\end{aligned} \tag{73}$$

where $x_1(t)$ and $y_1(t)$ govern the rapid discharges on the fast timescale, $x_2(t)$ and $y_2(t)$ govern SWEs on the intermediate timescale, $z(t)$ is the

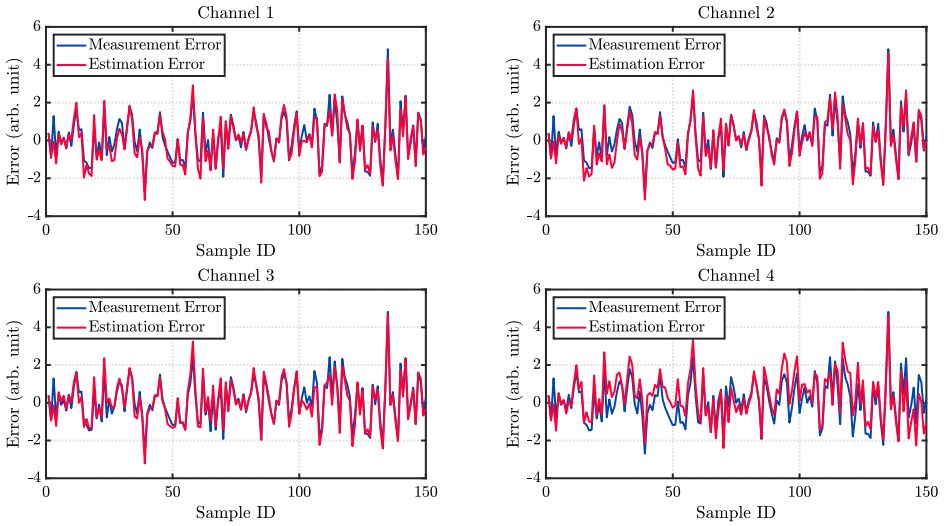

Fig. 8. Comparison between the measurement error of the υ-augmented system (with $\upsilon = 10$) versus the estimation error of a minimum-energy estimator implemented on the same, in the presence of process and measurement noises for 4 channels of a 64-channel EEG signal. (For interpretation of the references to color in this figure legend, the reader is referred to the web version of this article.).

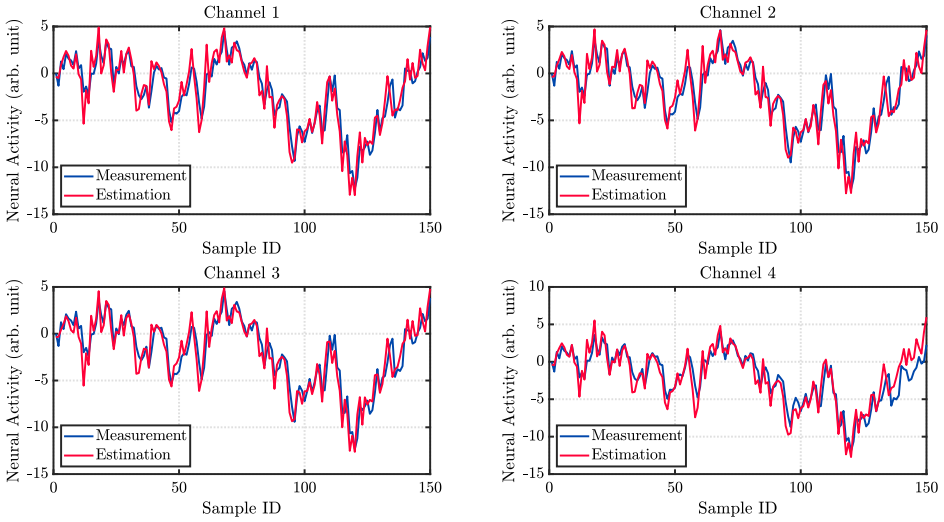

Fig. 9. Comparison between the measured output of the υ-augmented system (with $\upsilon = 20$) versus the estimated output of a minimum-energy estimator implemented on the same, in the presence of process and measurement noises for 4 channels of a 64-channel EEG signal. (For interpretation of the references to color in this figure legend, the reader is referred to the web version of this article.).

permittivity variable that operates on a slow timescale, $u(t)$ is a dummy variable that acts as a low-pass filter, x_0, y_0 are threshold constants, τ_0, τ_2 are time constants for the permittivity and the SWE-generating subsystems, respectively. Additionally, $I_{\text{rest},1}$ and $I_{\text{rest},2}$ are injection currents, γ is the time constant of the low-pass filter, and the functions f_1 and f_2 are defined as follows:

$$f_1(x_1, x_2, z) = \begin{cases} x_1^3 - 3x_1^2 & \text{when } x_1 < 0, \\ (x_2 - 0.6(z-4)^2)x_1 & \text{otherwise,} \end{cases} \tag{74}$$

and

$$f_2(x_2) = \begin{cases} 0 & \text{when } x_2 < -0.25, \\ 6(x_2 + 0.25) & \text{otherwise.} \end{cases} \tag{75}$$

Noise is introduced into each equation as linear additive white Gaussian noise with zero mean and a variance $\sigma_1^2 = 0.025$ for the first subsystem and $\sigma_2^2 = 0.25$ for the second subsystem. The descriptions along with the standard values of the parameters used in the Epileptor model are provided in Table 1. In what follows, we will use the simulated seizure data obtained by integrating the system (73) using the Euler–Maruyama method (Kloeden & Platen, 2013) with the standard values of the parameters provided in Table 1 and the initial conditions $(x_1(0), y_1(0), z(0), x_2(0), y_2(0), u(0)) = (0, -5, 3, 0, 0, 0)$ from the Epileptor model and then implement the proposed closed-loop MPC neuromodulation scheme on it.

To determine the parameters A and α that model both spatial coupling and fractional coefficients, respectively, that craft the evolution of the state dynamics in (70), we use the method proposed in Gupta et al. (2018a). Here, like the Jansen–Rit model, the system is SISO, and hence A and α are scalars. The parameters obtained are $A = -0.0051$ and $\alpha = 1.0614$. Furthermore, we assume that $B = 1$ and $B^w = 0.25$.

We implement the FOS-MPC neurostimulation strategy with $Q_k = I_n$, $R_k = I_{n_u}$, and $c_k = 0_{n_u \times 1}$ (with $n = n_u = 1$) and safety linear constraints of $-50 \le u[k] \le 50$. In this case, our predictive model was based on a $(p = 20)$–step predictive model approximation of the FOS plant, with a $(P = 20)$–step prediction horizon and $(M = 10)$–step control horizon. The results are presented in Fig. 13, which provide evidence that the proposed stimulation strategy allows us to achieve amplitude suppression for a seizure simulated by the Epileptor model with standard parameter values.

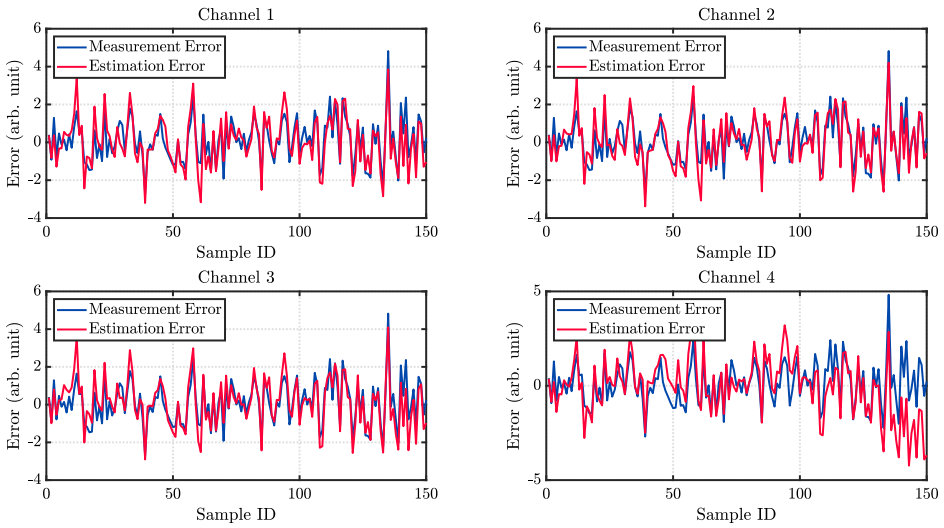

Fig. 10. Comparison between the measurement error of the υ-augmented system (with $\upsilon = 20$) versus the estimation error of a minimum-energy estimator implemented on the same, in the presence of process and measurement noises for 4 channels of a 64-channel EEG signal. (For interpretation of the references to color in this figure legend, the reader is referred to the web version of this article.).

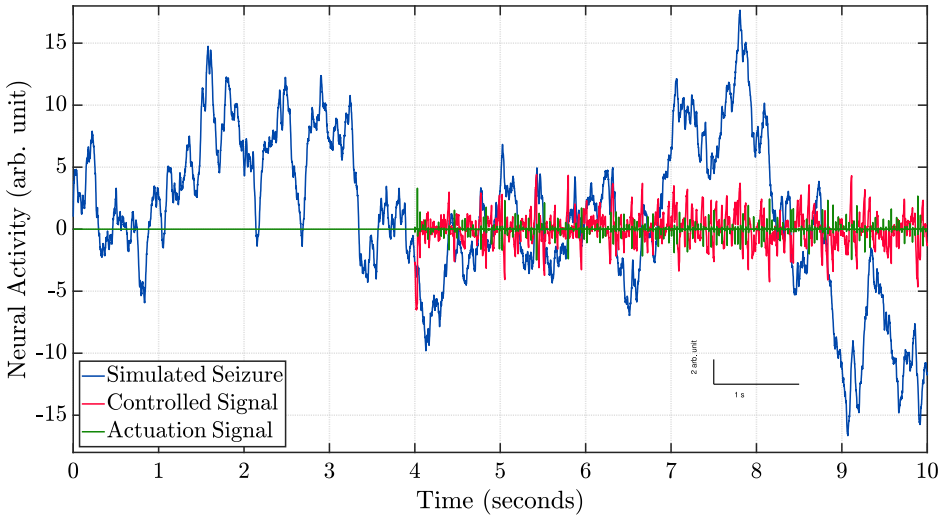

Fig. 11. Results of the proposed FOS-MPC closed-loop neurostimulation strategy on an iEEG seizure simulated by the Jansen–Rit neural mass model. The simulated iEEG signal with the seizure is depicted in blue, the controlled signal is depicted in red, and the stimulation pulses are shown in green. (For interpretation of the references to color in this figure legend, the reader is referred to the web version of this article.)

Table 1
Descriptions and standard parameter values of the Epileptor model.
Source: Adapted from Jirsa et al. (2014).

Parameters	Description	Values
x_0, y_0	Threshold constants	$x_0 = -1.6, y_0 = 1$
τ_0	Time constant of the permittivity variable	2857
τ_2	Time constant of the SWE-generating subsystem	10
$I_{\text{rest},1}, I_{\text{rest},2}$	Injection currents	$I_{\text{rest},1} = 3.1, I_{\text{rest},2} = 0.45$
γ	Time constant of the low-pass filter	0.01

15. Conclusions and directions for future research

Cyber-neural systems are becoming pervasive in today's society, yet they still lack the capability of performing real-time closed-loop control on neural activity. Control systems engineers will play a vital role in bringing this technology to reality as they develop the tools required by interdisciplinary teams involved in envisioning the next generation of neurotechnology.

That said, we provided a glance at some of the latest trends and techniques in fractional-order based system modeling, analysis, and closed-loop control towards the development of future neurotechnologies. In particular, we present results on system identification, state estimation, and closed-loop control for discrete-time fractional-order dynamical systems.

There are a plethora of interesting research directions that can be taken from here, which are pinpointed next.

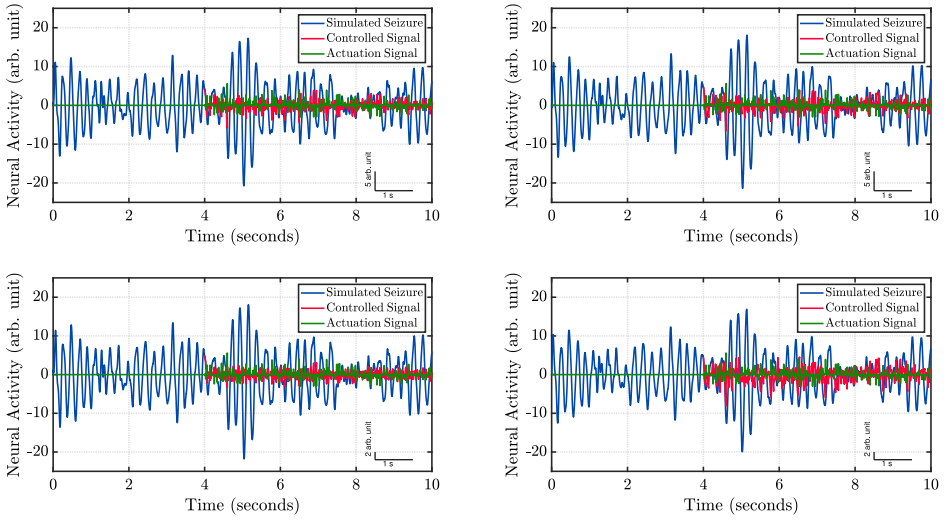

Fig. 12. Results of the proposed FOS-MPC closed-loop neurostimulation strategy on an iEEG seizure simulated by the traveling wave dynamics model proposed in Martinet et al. (2017). The simulated iEEG signal with the seizure is depicted in blue, the controlled signal is depicted in red, and the stimulation pulses are shown in green. (For interpretation of the references to color in this figure legend, the reader is referred to the web version of this article.)

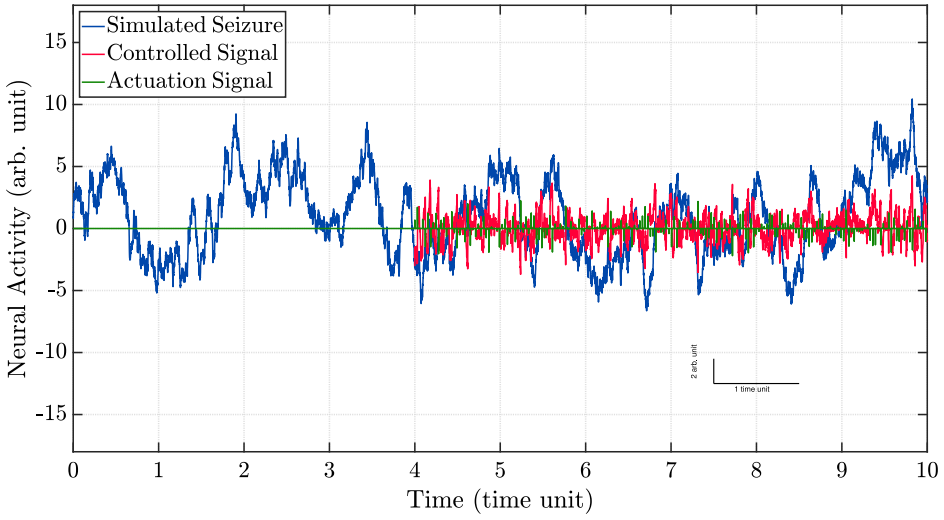

Fig. 13. Results of the proposed FOS-MPC closed-loop neurostimulation strategy on an iEEG seizure simulated by the Epileptor model. The simulated iEEG signal with the seizure is depicted in blue, the controlled signal is depicted in red, and the stimulation pulses are shown in green. (For interpretation of the references to color in this figure legend, the reader is referred to the web version of this article.)

System identification

System identification of fractional-order systems is an extremely under-explored field in general, with a lack of a systematic and unified theory, with some preliminary approaches utilizing wavelets (Flandrin, 1992), frequency-domain techniques (Adams, Hartley, & Lorenzo, 2006; Dzieliński et al., 2011), or a sequential combination of wavelets and expectation–maximization (EM) (Gupta et al., 2018a).

Although approaches using the EM algorithm for linear (Gibson & Ninness, 2005) as well as nonlinear system identification (Schön, Wills, & Ninness, 2011) have existed in the literature for a while now, one immediately notices that there is a long-standing problem in characterizing theoretical robustness guarantees for these approaches. We can draw inspiration from preliminary analyses of finite-sample robustness guarantees for EM in Balakrishnan, Wainwright, and Yu (2017), Wu, Yang, Zhao, and Zhu (2016), Yan, Yin, and Sarkar (2017) to characterize the sample complexity in identifying linear time-invariant (LTI) systems and do the same for fractional-order systems.

In practice, it would be important to investigate approaches to identify the spatial and temporal parameters of fractional-order systems based on bootstrapping (Tjärnström, 1999), which uses an alternating scheme to obtain progressively better identifications of the parameters. Future work should focus on chalking out a general theory that identifies certain classes of fractional-order systems.

Alternatively, one could also look into strategies behind using recurrent neural networks (RNNs) to identify the fractional-order systems' parameters. One of the most celebrated results in neural network theory, the *universal approximation theorem* (Cybenko, 1989; Funahashi, 1989; Hornik, Stinchcombe, & White, 1989), states that continuous functions can be arbitrarily well-approximated by single-hidden-layer feedforward neural networks. While recent work (Hutter, Gül, & Bölcskei, 2021) seems to suggest the presence of allied results when RNNs are used to identify stable LTI systems optimally in the sense of metric entropy (Zames & Owen, 1993), it remains to be seen whether universal approximation theorem-like results can be derived when RNNs are used to identify fractional-order systems.

It would also be interesting to investigate fundamental information-theoretic connections between the number of samples needed to perform online system identification for fractional-order systems that would, in turn, allow for a more robust control design

using the same number of samples. Furthermore, one could also potentially look into the number of samples needed to uniquely identify the parameters of fractional-order systems and whether different identified realizations potentially correspond to different fractional-order systems.

State estimation

Although fractional-order systems have found vast success in modeling the spatiotemporal properties of EEG signals, some of the properties accounted for by these models actually originate from unknown sources external to the system under consideration. Future work should focus on modeling these external sources by unknown input stimuli and then focus on state estimation of the resultant model with unknown inputs.

Real-time neural activity can be monitored to self-regulate brain function. This is known in the literature as neurofeedback (Marzbani, Marateb, & Mansourian, 2016), and it would be interesting to study how the introduction of feedback to such a system changes our perspectives on this problem.

While the construction of resilient state estimators has grown over the last decade, little effort has been put in developing resilient versions of state estimators for fractional-order systems. In particular, assuming that the disturbance and noise distributions do not follow a Gaussian distribution, it is imperative to build a resilient and attack-resistant version of the minimum-energy state estimator. Specifically, it is important to consider adversarial attacks or artifacts associated with the measurement process since adversarial attacks on sensors often do not follow any particular dynamic or stochastic characterization.

Last but not least, it is crucial to understand how to design filter-like methods that solve the problems of simultaneous system identification and state estimation suitable for the deployment in real-time CNS.

Closed-loop control

Very rarely in practical settings do we have deterministic fractional-order models. As we saw, neural signals are particularly prone to artifacts from outside the brain. Furthermore, stabilizing the underlying models in the presence of disturbances becomes relevant in the treatment of disorders like epilepsy, Parkinson's, or Alzheimer's disease.

In recent years, there have been increasing research efforts into finding possible therapies for the aforementioned diseases using neurofeedback (Marzbani et al., 2016). Future work, therefore, should focus on developing controllers and observers for fractional-order systems with the associated process and measurement noise as well as investigating the possible existence of separation principle-like results akin to those already existing in the field of linear stochastic control theory.

Another direction of work entails deriving robustness guarantees for controlling discrete-time fractional-order systems using an inner-outer loop control strategy. Specifically, in this context, we seek to discover the advantages and disadvantages of truncating a discrete-time fractional-order systems according to a given truncation horizon, thus approximating the fractional-order systems as an augmented LTI system and performing model predictive control.

Additionally, one could also rely on some tools from robust control, namely integral quadratic constraints (IQCs) (Megretski & Rantzer, 1997). IQCs are, essentially, inequalities used to describe possible input–output signals resulting from a system component that is challenging to model because it is either nonlinear, time-varying, noisy, or switch stochastically or adversarially with time. A particular issue of interest is to explore the trade-offs in performance when fractional-order systems (which represents the inner loop) are written as an augmented LTI system due to a fixed truncation horizon versus when they are modeled as a non-Markovian nonlinearity with IQCs.

Additionally, although finite-time LTI truncations of fractional-order systems with constant truncation horizons are considered in this paper, fractional-order systems inherently possess infinite long-term memory. The question becomes whether the theory of linear control systems in infinite dimensions (Curtain & Zwart, 2012) can be used to provide key insights into control-theoretic properties such as controllability, observability, and stabilizability for such systems. While there have been some preliminary works in this direction (Baleanu, Fedorov, Gordievskikh, & Taş, 2019; Sabatier, 2021; Wei, Chen, Wang, & Wang, 2019; Zitane, Boutoulout, & Torres, 2020), further investigation is needed. Consequently, future work of fractional-order systems must use mathematical techniques previously applied to analyze partial and delay differential equations, in particular, operator equations and C_0-semigroup theory (Bamieh, Paganini, & Dahleh, 2002).

From an engineering or applied control point-of-view, it is important to pinpoint some limitations and drawbacks of current event-triggered open-loop stimulation strategies (i.e., they can be inefficient or even cause seizure-like activity). Consequently, it serves as a call to action for neurophysiologists and engineers that work with neurostimulation (as well as deep brain stimulation) devices, to validate *in vitro* and *in vivo* scenarios. That said, the advances in computational processing power made in the last 10–20 years have made the prospects of turning ideas that were theoretically devised and previously impossible to implement in real-life into realizable technology. MPC and fractional-order systems-based technologies both fall under this category and have thus been significantly overlooked in the industry. However, both are growing in popularity amongst several research communities, and some predict a considerably more widespread impact than originally thought.

Despite this promising outlook, validation is insufficient to establish a framework since several foundational problems still need to be addressed. Specifically, determining the robustness of the stimulation strategies concerning the parameters of the models (e.g., the dynamics and the stimuli deployed, as well as the approximations considered to attain real-time stimulation) in devices with low storage, and limited battery and computation capabilities. Towards this goal, only interdisciplinary work between scientists and engineers will lead to the necessary success that ultimately will be reflected in the improvement of the quality of life for patients with neurological disorders (e.g., epilepsy).

Declaration of competing interest

The authors declare that they have no known competing financial interests or personal relationships that could have appeared to influence the work reported in this paper.

References

Adams, J. L., Hartley, T. T., & Lorenzo, C. F. (2006). Fractional-order system identification using complex order-distributions. In *Proceedings of the 2nd IFAC Workshop on Fractional Differentiation and its Applications, vol. 39* (11), (pp. 200–205). Porto, Portugal.

Agrawal, O. P. (2002). Formulation of Euler–Lagrange equations for fractional variational problems. *Journal of Mathematical Analysis and Applications*, *272*(1), 368–379.

Agrawal, O. P. (2004). A general formulation and solution scheme for fractional optimal control problems. *Nonlinear Dynamics*, *38*(1), 323–337.

Agrawal, O. P., & Baleanu, D. (2007). A Hamiltonian formulation and a direct numerical scheme for fractional optimal control problems. *Journal of Vibration and Control*, *13*(9–10), 1269–1281.

Agrawal, O. P., Defterli, O., & Baleanu, D. (2010). Fractional optimal control problems with several state and control variables. *Journal of Vibration and Control*, *16*(13), 1967–1976.

Aguiar, A. P., & Hespanha, J. P. (2006). Minimum-energy state estimation for systems with perspective outputs. *IEEE Transactions on Automatic Control*, *51*(2), 226–241.

Alessandretti, A., Aguiar, A. P., Hespanha, J. P., & Valigi, P. (2011). A minimum energy solution to monocular simultaneous localization and mapping. In *Proceedings 50th IEEE Conference on Decision and Control held jointly with the European Control Conference* (pp. 4566–4571). Orlando, FL, USA.

Alessandretti, A., Pequito, S., Pappas, G. J., & Aguiar, A. P. (2020). Finite-dimensional control of linear discrete-time fractional-order systems. *Automatica*, *115*.

Almeida, R., & Torres, D. F. (2015). A discrete method to solve fractional optimal control problems. *Nonlinear Dynamics*, *80*(4), 1811–1816.

Ashourvan, A., et al. (2020). Model-based design for seizure control by stimulation. *Journal of Neural Engineering*, *17*(2).

Balachandran, K., Govindaraj, V., Ortigueira, M. D., Rivero, M., & Trujillo, J. J. (2013). Observability and controllability of fractional linear dynamical systems. *IFAC Proceedings Volumes*, *46*(1), 893–898.

Balakrishnan, S., Wainwright, M. J., & Yu, B. (2017). Statistical guarantees for the EM algorithm: From population to sample-based analysis. *The Annals of Statistics*, *45*(1), 77–120.

Baleanu, D., Defterli, O., & Agrawal, O. P. (2009). A central difference numerical scheme for fractional optimal control problems. *Journal of Vibration and Control*, *15*(4), 583–597.

Baleanu, D., Diethelm, K., Scalas, E., & Trujillo, J. J. (2012). *Fractional calculus: models and numerical methods, vol. 3*. World Scientific.

Baleanu, D., Fedorov, V. E., Gordievskikh, D. M., & Taş, K. (2019). Approximate controllability of infinite-dimensional degenerate fractional order systems in the sectorial case. *Mathematics*, *7*(8).

Baleanu, D., Güvenç, Z. B., Machado, J. T., et al. (2010). *New trends in nanotechnology and fractional calculus applications*. Springer.

Baleanu, D., Machado, J. A. T., & Luo, A. C. (2011). *Fractional dynamics and control*. New York, NY, USA: Springer.

Bamieh, B., Paganini, F., & Dahleh, M. A. (2002). Distributed control of spatially invariant systems. *IEEE Transactions on Automatic Control*, *47*(7), 1091–1107.

Bargmann, C., Newsome, W., Anderson, A., Brown, E., Deisseroth, K., Donoghue, J., et al. (2014). Brain 2025: a scientific vision. In *Brain research through advancing innovative neurotechnologies (BRAIN) Working group report to the advisory committee to the director, NIH*. National Institutes of Health Bethesda, MD.

Bassett, D. S., & Sporns, O. (2017). Network neuroscience. *Nature Neuroscience*, *20*(3), 353–364.

Battaglia, J.-L., Le Lay, L., Batsale, J.-C., Oustaloup, A., & Cois, O. (2000). Heat flux estimation through inverted non-integer identification models; Utilisation de modeles d'identification non entiers pour la resolution de problemes inverses en conduction. *International Journal of Thermal Sciences*, *39*.

Bennett, S. (2001). The past of PID controllers. *Annual Reviews in Control*, *25*, 43–53.

Benzaouia, A., Hmamed, A., Mesquine, F., Benhayoun, M., & Tadeo, F. (2014). Stabilization of continuous-time fractional positive systems by using a Lyapunov function. *IEEE Transactions on Automatic Control*, *59*(8), 2203–2208.

Bequette, B. W. (2013). Algorithms for a closed-loop artificial pancreas: The case for model predictive control. *Journal of Diabetes Science and Technology*, *7*(6), 1632–1643. http://dx.doi.org/10.1177/193229681300700624.

Birs, I., Muresan, C., Nascu, I., & Ionescu, C. (2019). A survey of recent advances in fractional order control for time delay systems. *IEEE Access*, *7*, 30951–30965.

Biswas, R. K., & Sen, S. (2011). Fractional optimal control problems with specified final time. *Journal of Computational and Nonlinear Dynamics*, *6*(2).

Bogdan, P. (2015). Mathematical modeling and control of multifractal workloads for data-center-on-a-chip optimization. In *Proceedings of the 9th International symposium on networks-on-chip* (pp. 1–8).

Bogdan, P., Jain, S., Goyal, K., & Marculescu, R. (2012). Implantable pacemakers control and optimization via fractional calculus approaches: A cyber-physical systems perspective. In *2012 IEEE/ACM Third International conference on cyber-physical systems* (pp. 23–32). IEEE.

Bogdan, P., Jain, S., & Marculescu, R. (2013). Pacemaker control of heart rate variability: A cyber physical system perspective. *ACM Transactions on Embedded Computing Systems (TECS)*, *12*(1s), 1–22.

Bogdan, P., & Marculescu, R. (2011). Towards a science of cyber-physical systems design. In *2011 IEEE/ACM Second international conference on cyber-physical systems* (pp. 99–108). IEEE.

Bogdan, P., Marculescu, R., & Jain, S. (2013). Dynamic power management for multidomain system-on-chip platforms: An optimal control approach. *ACM Transactions on Design Automation of Electronic Systems (TODAES)*, *18*(4), 1–20.

Bogdan, P., Marculescu, R., Jain, S., & Gavila, R. T. (2012). An optimal control approach to power management for multi-voltage and frequency islands multiprocessor platforms under highly variable workloads. In *2012 IEEE/ACM Sixth international symposium on networks-on-chip* (pp. 35–42). IEEE.

Bonilla, B., Rivero, M., Rodríguez-Germá, L., & Trujillo, J. J. (2007). Fractional differential equations as alternative models to nonlinear differential equations. *Applied Mathematics and Computation*, *187*(1), 79–88.

Bonnabel, S., & Slotine, J.-J. (2015). A contraction theory-based analysis of the stability of the deterministic extended Kalman filter. *IEEE Transactions on Automatic Control*, *60*(2), 565–569.

Buchstaller, D., Liu, J., & French, M. (2020). The deterministic interpretation of the Kalman filter. *International Journal of Control*, http://dx.doi.org/10.1080/00207179.2020.1755895.

Busłowicz, M., & Ruszewski, A. (2013). Necessary and sufficient conditions for stability of fractional discrete-time linear state-space systems. *Bulletin of the Polish Academy of Sciences. Technical Sciences*, *61.4*(4).

Cao, Y., Li, Y., Ren, W., & Chen, Y. (2009). Distributed coordination of networked fractional-order systems. *IEEE Transactions on Systems, Man and Cybernetics, Part B (Cybernetics)*, *40*(2), 362–370.

Cao, Q., Ramos, G., Bogdan, P., & Pequito, S. (2019). The actuation spectrum of spatiotemporal networks with power-law time dependencies. *Advances in Complex Systems*, *22*(07n08), Article 1950023.

Caponetto, R. (2010). *Fractional order systems: modeling and control applications, vol. 72*. World Scientific.

Carmena, J., Sajda, P., & Robinson, J. (2019). Future neural therapeutics: Closed-loop control of neural activity technology roadmap white paper. *IEEE Brain Initiative*, 1–28.

Chatterjee, S., Alessandretti, A., Aguiar, A. P., & Pequito, S. (2021). Discrete-time fractional-order dynamical networks minimum-energy state estimation. arXiv preprint arXiv:2104.09409.

Chatterjee, S., & Pequito, S. (2019). Dealing with state estimation in fractional-order systems under artifacts. In *Proceedings of the 2019 American control conference* (pp. 878–883). IEEE.

Chatterjee, S., & Pequito, S. (2022). On learning discrete-time fractional-order dynamical systems. In *To Appear in 2022 American Control Conference*. arXiv preprint arXiv:2103.14975.

Chatterjee, S., Romero, O., Ashourvan, A., & Pequito, S. (2020). Fractional-order model predictive control as a framework for electrical neurostimulation in epilepsy. *Journal of Neural Engineering*, *17*(6).

Chatterjee, S., Romero, O., & Pequito, S. (2019). A separation principle for discrete-time fractional-order dynamical systems and its implications to closed-loop neurotechnology. *IEEE Control System Letters*, *3*(3), 691–696. http://dx.doi.org/10.1109/LCSYS.2019.2917164.

Chavarriaga, R. (2020). *Standards roadmap: Neurotechnologies for brain-machine interfacing*. IEEE.

Chen, Y. (2010). Fractional calculus, delay dynamics and networked control systems. In *Proceedings of the 2010 3rd International symposium on resilient control systems* (pp. 58–63). IEEE.

Chen, Y., Ahn, H.-S., & Podlubny, I. (2005). Robust stability check of fractional order linear time invariant systems with interval uncertainties. In *IEEE International conference mechatronics and automation, 2005, vol. 1* (pp. 210–215). IEEE.

Chen, Y., Moore, K. L., Vinagre, B. M., & Podlubny, I. (2004). Robust PID controller autotuning with a phase shaper. In *First IFAC workshop on fractional differentiation and its applications* (pp. 162–167). Citeseer.

Chen, Y., Petras, I., & Xue, D. (2009). Fractional order control-a tutorial. In *2009 American Control Conference* (pp. 1397–1411). IEEE.

Chen, W., Sun, H., Zhang, X., & Korošak, D. (2010). Anomalous diffusion modeling by fractal and fractional derivatives. *Computers & Math. with Appl.*, *59*(5), 1754–1758.

Curtain, R. F., & Zwart, H. (2012). *An introduction to infinite-dimensional linear systems theory, vol. 21*. New York, NY, USA: Springer-Verlag.

Cybenko, G. (1989). Approximation by superpositions of a sigmoidal function. *Mathematics of Control, Signals, and Systems*, *2*(4), 303–314.

Dastjerdi, A. A., Vinagre, B. M., Chen, Y., & HosseinNia, S. H. (2019). Linear fractional order controllers; a survey in the frequency domain. *Annual Reviews in Control*, *47*, 51–70.

Diethelm, K. (2010). *The analysis of fractional differential equations: an application-oriented exposition using differential operators of caputo type*. Springer Science & Business Media.

Duhé, J.-F., Victor, S., Melchior, P., Abdelmounen, Y., & Roubertie, F. (2022). Modeling thermal systems with fractional models: human bronchus application. *Nonlinear Dynamics*, 1–17.

Dzielinski, A., & Sierociuk, D. (2005). Adaptive feedback control of fractional order discrete state-space systems. In *Proceedings of the International Conference on Computational Intelligece for Modelelling, Control and Automation, and International Conference on Intelligent Agents, Web Technologies and Internet Commerce, vol. 1* (pp. 804–809). Vienna, Austria.

Dzieliński, A., & Sierociuk, D. (2008). Stability of discrete fractional order state-space systems. *Journal of Vibration and Control*, *14*(9–10), 1543–1556.

Dzieliński, A., Sierociuk, D., Sarwas, G., Petráš, I., Podlubny, I., & Škovránek, T. (2011). Identification of the fractional-order systems: A frequency domain approach. *Acta Montanistica Slovaca*, *16*(1), 26–33.

Eddine, A. N., Huard, B., Gabano, J.-D., & Poinot, T. (2018). Initialization of a fractional order identification algorithm applied for lithium-ion battery modeling in time domain. *Communications in Nonlinear Science and Numerical Simulation*, *59*, 375–386.

Efe, M. O. (2011). Fractional order systems in industrial automation—a survey. *IEEE Transactions on Industrial Informatics*, *7*(4), 582–591.

Fagnani, F., & Willems, J. C. (1997). Deterministic Kalman filtering in a behavioral framework. *System & Control Letters*, *32*(5), 301–312.

Fairclough, S. H., & Lotte, F. (2020). Grand challenges in neurotechnology and system neuroergonomics. *Frontiers in Neuroergonomics*, *1*, 2.

Flandrin, P. (1992). Wavelet analysis and synthesis of fractional Brownian motion. *IEEE Transactions on Information Theory*, *38*(2), 910–917.

Fleming, W. H. (1997). Deterministic nonlinear filtering. *Annali Della Scuola Normale Superiore Di Pisa, Classe Di Scienze, Ser. 4, 25*(3–4), 435–454.

Foucart, S., & Rauhut, H. (2013). *Applied and Numerical Harmonic Analysis, A Mathematical Introduction To Compressive Sensing* (pp. I–XVIII, 1–625). New York, NY, USA: Birkhäuser.

Frederico, G. S., & Torres, D. F. (2007). A formulation of Noether's theorem for fractional problems of the calculus of variations. *Journal of Mathematical Analysis and Applications*, *334*(2), 834–846.

Frederico, G. S., & Torres, D. F. (2008). Fractional conservation laws in optimal control theory. *Nonlinear Dynamics*, *53*(3), 215–222.

Funahashi, K.-I. (1989). On the approximate realization of continuous mappings by neural networks. *Neural Networks*, *2*(3), 183–192.

Gabano, J.-D., Poinot, T., & Kanoun, H. (2011). Identification of a thermal system using continuous linear parameter-varying fractional modelling. *IET Control Theory & Applications*, *5*(7), 889–899.

Ghorbani, M., & Bogdan, P. (2013). A cyber-physical system approach to artificial pancreas design. In *Proc. 9th IEEE/ACM/IFIP Int. conf. hardware/software codesign and syst. synthesis* (pp. 1–10). Montreal, QC, Canada.

Ghorbani, M., & Bogdan, P. (2014). Reducing risk of closed loop control of blood glucose in artificial pancreas using fractional calculus. In *2014 36th Annual International Conference of the IEEE Engineering in Medicine and Biology Society* (pp. 4839–4842). IEEE.

Ghorbani, M., Wang, Y., Xue, Y., Pedram, M., & Bogdan, P. (2014). Prediction and control of bursty cloud workloads: a fractal framework. In *Proceedings of the 2014 International conference on hardware/software codesign and system synthesis* (pp. 1–9).

Gibson, S., & Ninness, B. (2005). Robust maximum-likelihood estimation of multivariable dynamic systems. *Automatica*, *41*(10), 1667–1682.

Goldberger, A. L., et al. (2000). PhysioBank, PhysioToolkit, And PhysioNet: Components of a new research resource for complex physiologic signals. *Circulation*, *101*(23), e215–e220.

Goodrich, C., & Peterson, A. C. (2015). *Discrete fractional calculus, vol. 1350*. Springer.

Grant, M., & Boyd, S. (2008). Graph implementations for nonsmooth convex programs. In V. Blondel, S. Boyd, & H. Kimura (Eds.), *Lecture notes in control and information sciences*, *Recent advances in learning and control* (pp. 95–110). London, United Kingdom: Springer.

Grant, M., & Boyd, S. (2014). CVX: Matlab software for disciplined convex programming, version 2.1. http://cvxr.com/cvx. (Accessed 18 July 2021).

Guermah, S., Djennoune, S., & Bettayeb, M. (2008). Controllability and observability of linear discrete-time fractional-order systems. *International Journal of Applied Mathematics & Computer Science*, *18*(2).

Gupta, G., Pequito, S., & Bogdan, P. (2018a). Dealing with unknown unknowns: Identification and selection of minimal sensing for fractional dynamics with unknown inputs. In *Proceedings of the 2018 American Control Conference* (pp. 2814–2820). Milwaukee, WI, USA.

Gupta, G., Pequito, S., & Bogdan, P. (2018b). Re-thinking EEG-based non-invasive brain interfaces: Modeling and analysis. In *Proceedings of the ACM/IEEE 9th Internation conference on cyber-physical systems* (pp. 275–286). Porto, Portugal.

Gupta, G., Pequito, S., & Bogdan, P. (2019). Learning latent fractional dynamics with unknown unknowns. In *Proceedings of the 2019 American Control Conference* (pp. 217–222). IEEE.

Gupta, G., Yin, C., Deshmukh, J. V., & Bogdan, P. (2021). Non-markovian reinforcement learning using fractional dynamics. In *2021 60th IEEE Conference on Decision and Control* (pp. 1542–1547). IEEE.

Ha, T. N., & Aguiar, A. P. (2018). Cooperative joint estimation and localization using mobile multi-agent systems: A minimum energy estimator approach. In *Proceedings 16th European Control Conference* (pp. 2224–2229). Limassol, Cyprus.

Haring, M., & Johansen, T. A. (2020). On the stability bounds of Kalman filters for linear deterministic discrete-time systems. *IEEE Transactions on Automatic Control*, *65*(10), 4434–4439. http://dx.doi.org/10.1109/TAC.2020.2966150.

Hassani, V., Aguiar, A. P., Athans, M., & Pascoal, A. M. (2009). Multiple model adaptive estimation and model identification using a minimum energy criterion. In *Proceedings 2009 American Control Conference* (pp. 518–523). St. Louis, MO, USA.

Hijab, O. (1980). *Minimum energy estimation* (Ph.D. thesis), Berkeley: Univ. California.

Hornik, K., Stinchcombe, M., & White, H. (1989). Multilayer feedforward networks are universal approximators. *Neural Networks*, *2*(5), 359–366.

Hutter, C., Gül, R., & Bölcskei, H. (2021). Metric entropy limits on recurrent neural network learning of linear dynamical systems. arXiv:2105.02556.

Insel, T. R., Landis, S. C., & Collins, F. S. (2013). The NIH brain initiative. *Science*, *340*(6133), 687–688.

Jansen, B. H., & Rit, V. G. (1995). Electroencephalogram and visual evoked potential generation in a mathematical model of coupled cortical columns. *Biological Cybernetics*, *73*(4), 357–366.

Jansen, B. H., Zouridakis, G., & Brandt, M. E. (1993). A neurophysiologically-based mathematical model of flash visual evoked potentials. *Biological Cybernetics*, *68*(3), 275–283.

Jean-Claude, T., Nezha, M., & Alain, O. (2013). The Caputo derivative and the infinite state approach. *IFAC Proceedings Volumes*, *46*(1), 587–592.

Jirsa, V. K., Stacey, W. C., Quilichini, P. P., Ivanov, A. I., & Bernard, C. (2014). On the nature of seizure dynamics. *Brain*, *137*(8), 2210–2230.

Khambhati, A. N., Davis, K. A., Oommen, B. S., Chen, S. H., Lucas, T. H., Litt, B., et al. (2015). Dynamic network drivers of seizure generation, propagation and termination in human neocortical epilepsy. *PLoS Computational Biology*, *11*(12).

Kilbas, A. A., Srivastava, H. M., & Trujillo, J. J. (2006). *Theory and applications of fractional differential equations, vol. 204*. elsevier.

Kilbas, A., & Trujillo, J. (2001). Differential equations of fractional order: methods results and problem—I. *Applicable Analysis*, *78*(1–2), 153–192.

Kilbas, A., & Trujillo, J. (2002). Differential equations of fractional order: methods, results and problems. II. *Applicable Analysis*, *81*(2), 435–493.

Kloeden, P. E., & Platen, E. (2013). *Numerical solution of stochastic differential equations, vol. 23*. Berlin, Heidelberg, Germany: Springer-Verlag.

Kokotovic, P. V. (1992). The joy of feedback: nonlinear and adaptive. *IEEE Control Systems Magazine*, *12*(3), 7–17.

Krener, A. J. (2003). The convergence of the minimum energy estimator. In W. Kang, M. Xiao, & C. Borges (Eds.), *New trends in nonlinear dyn. and control and their appl., vol. 295* (pp. 187–208). Berlin, Heidelberg, Germany: Springer-Verlag.

Kyriakis, P., Pequito, S., & Bogdan, P. (2020). On the effects of memory and topology on the controllability of complex dynamical networks. *Scientific Reports*, *10*(1), 1–13.

Lanusse, P., Malti, R., & Melchior, P. (2013). CRONE control system design toolbox for the control engineering community: tutorial and case study. *Philosophical Transactions of the Royal Society of London A (Mathematical and Physical Sciences)*, *371*(1990), Article 20120149.

LeDoux, J. (1998). *The emotional brain: the mysterious underpinnings of emotional life*. Simon and Schuster.

Lewis, T. (2020). Elon Musk's pig-brain implant is still a long way from 'Solving paralysis'. *Scientific American*, online.

Li, Y., Chen, Y., & Podlubny, I. (2009). Mittag–Leffler stability of fractional order nonlinear dynamic systems. *Automatica*, *45*(8), 1965–1969.

Li, Y., Chen, Y., & Podlubny, I. (2010). Stability of fractional-order nonlinear dynamic systems: Lyapunov direct method and generalized Mittag–Leffler stability. *Computers & Mathematics with Applications*, *59*(5), 1810–1821.

Li, A., Inati, S., Zaghloul, K., & Sarma, S. (2017). Fragility in epileptic networks: the epileptogenic zone. In *2017 American Control Conference* (pp. 2817–2822). IEEE.

Lozano, R., Brogliato, B., et al. (1992). Adaptive control of robot manipulators with flexible joints. *IEEE Transactions on Automatic Control*, *37*(2), 174–181.

Lundstrom, B. N., Higgs, M. H., Spain, W. J., & Fairhall, A. L. (2008). Fractional differentiation by neocortical pyramidal neurons. *Nature Neuroscience*, *11*(11), 1335–1342.

Magin, R. L. (2006). *Fractional calculus in bioengineering*. Redding, CT, USA: Begell House.

Mahmoud, M. (2012). *Advances in discrete time systems*. BoD–Books on Demand.

Malti, R., & Victor, S. (2015). CRONE toolbox for system identification using fractional differentiation models. *IFAC-PapersOnLine*, *48*(28), 769–774.

Markram, H. (2012). The human brain project. *Scientific American*, *306*(6), 50–55.

Martinet, L.-E., et al. (2017). Human seizures couple across spatial scales through travelling wave dynamics. *Nature Communications*, *8*.

Marzbani, H., Marateb, H. R., & Mansourian, M. (2016). Neurofeedback: A comprehensive review on system design, methodology and clinical applications. *Basic and Clinical Neuroscience*, *7*(2), 143–158.

Matignon, D. (1996). Stability results for fractional differential equations with applications to control processing. *Computational Engineering in Systems Applications*, *2*(1), 963–968.

Matignon, D., & d'Andréa Novel, B. (1996). Some results on controllability and observability of finite-dimensional fractional differential systems. *Computational Engineering in Systems Applications*, *2*, 952–956.

Matušů, R. (2011). Application of fractional order calculus to control theory. *International Journal of Mathematical Models and Methods in Applied Sciences*, *5*(7), 1162–1169.

Mayoufi, A., Victor, S., Chetoui, M., Malti, R., & Aoun, M. (2021). Output error MISO system identification using fractional models. *Fractional Calculus & Applied Analysis*, *24*(5), 1601–1618.

Megretski, A., & Rantzer, A. (1997). System analysis via integral quadratic constraints. *IEEE Transactions on Automatic Control*, *42*(6), 819–830.

Melchior, P., Orsoni, B., Lavialle, O., & Oustaloup, A. (2001). The CRONE toolbox for matlab: fractional path planning design in robotics. In *Proceedings 10th IEEE International Workshop on Robot and Human Interactive Communication. ROMAN 2001 (Cat. No. 01TH8591)* (pp. 534–540). IEEE.

Melchior, P., Pellet, M., Petit, J., Cabelguen, J.-M., & Oustaloup, A. (2012). Analysis of muscle length effect on an s type motor-unit fractional multi-model. *Signal, Image and Video Processing*, *6*(3), 421–428.

Miljković, N., Popović, N., Djordjević, O., Konstantinović, L., & Šekara, T. B. (2017). ECG Artifact cancellation in surface EMG signals by fractional order calculus application. *Computer Methods and Programs in Biomedicine*, *140*, 259–264.

Monje, C. A., Chen, Y., Vinagre, B. M., Xue, D., & Feliu-Batlle, V. (2010). *Fractional-order systems and controls: fundamentals and applications*. Springer Science & Business Media.

Monje, C. A., Vinagre, B. M., Feliu, V., & Chen, Y. (2008). Tuning and auto-tuning of fractional order controllers for industry applications. *Control Engineering Practice*, *16*(7), 798–812.

Moon, F. C. (2008). *Chaotic and fractal dynamics: an introduction for applied scientists and engineers*. Hoboken, NJ, USA: Wiley.

Moratti, S., & Patterson, D. (2014). Adverse psychological effects to deep brain stimulation: Overturning the question. *American Journal of Bioethics Neuroscience*, *5*(4), 62–64.

Mortensen, R. E. (1968). Maximum-likelihood recursive nonlinear filtering. *Journal of Optimization Theory and Applications*, *2*(6), 386–394.

Mozyrska, D., & Pawłuszewicz, E. (2012). Fractional discrete-time linear control systems with initialisation. *International Journal of Control*, *85*(2), 213–219.

NAE (2022). Grand challenges - reverse-engineer the brain. URL http://www.engineeringchallenges.org/challenges/9109.aspx.

Najar, S., Abdelkrim, M. N., Abdelhamid, M., & Mohamed, A. (2009). Discrete fractional Kalman filter. In *Proc. 2nd IFAC Conf. intell. control syst. signal process., vol. 42* (19), (pp. 520–525). Istanbul, Turkey.

Narang, A., Shah, S. L., & Chen, T. (2011). Continuous-time model identification of fractional-order models with time delays. *IET Control Theory & Applications*, *5*(7), 900–912.

Nemati, S., Lima, P. M., & Torres, D. F. (2019). A numerical approach for solving fractional optimal control problems using modified hat functions. *Communications in Nonlinear Science and Numerical Simulation*, *78*, Article 104849.

Oldham, K., & Spanier, J. (1974). *The fractional calculus theory and applications of differentiation and integration to arbitrary order*. Elsevier.

Ortigueira, M. D. (2000). Introduction to fractional linear systems. Part 1: Continuous-time case. *IEE Proceedings-Vision, Image and Signal Processing*, *147*(1), 62–70.

Oustaloup, A., Levron, F., Victor, S., & Dugard, L. (2021). Non-integer (or fractional) power model of a viral spreading: application to the COVID-19. arXiv preprint arXiv:2102.13471.

Oustaloup, A., Melchior, P., Lanusse, P., Cois, O., & Dancla, F. (2000). The CRONE toolbox for matlab. In *Conference Proceedings IEEE International Symposium on Computer-Aided Control System Design (Cat. No. 00TH8537)* (pp. 190–195). IEEE.

Oustaloup, A., Sabatier, J., Lanusse, P., Malti, R., Melchior, P., Moreau, X., et al. (2008). An overview of the CRONE approach in system analysis, modeling and identification, observation and control. *IFAC Proceedings Volumes*, *41*(2), 14254–14265.

Pequito, S., Aguiar, A. P., & Gomes, D. A. (2009). The entropy penalized minimum energy estimator. In *Proceedings 48th IEEE Conference on Decision and Control held jointly with the 28th Chinese Control Conference* (pp. 1285–1290). Shanghai, China.

Pequito, S., Ashourvan, A., Bassett, D., Litt, B., & Pappas, G. J. (2017). Spectral control of cortical activity. In *2017 American Control Conference* (pp. 2785–2791). IEEE.

Pequito, S., Bogdan, P., & Pappas, G. J. (2015). Minimum number of probes for brain dynamics observability. In *Proceedings 54th IEEE Conference on Decision and Control* (pp. 306–311). Osaka, Japan: http://dx.doi.org/10.1109/CDC.2015.7402218.

Petráš, I. (2011). Fractional-order chaotic systems. In *Fractional-order nonlinear systems: modeling, analysis and simulation* (pp. 103–184). Berlin, Heidelberg, Germany: Springer-Verlag.

Petráš, I. (2021). Novel fractional-order model predictive control: State-space approach. *IEEE Access*, *9*, 92769–92775.

Podlubny, I. (1998). *Fractional differential equations: an introduction to fractional derivatives, fractional differential equations, to methods of their solution and some of their applications*. Elsevier.

Podlubny, I. (1999). Fractional-order systems and $PI^{\lambda}D^{\mu}$-controllers. *IEEE Transactions on Automatic Control*, *44*(1), 208–214.

Presigny, C., & Fallani, F. D. V. (2021). Multiscale modeling of brain network organization. arXiv preprint arXiv:2111.13473.

Qin, S. J., & Badgwell, T. A. (2003). A survey of industrial model predictive control technology. *Control Engineering Practice*, *11*(7), 733–764.

Reed, E. A., Bogdan, P., & Pequito, S. (2021). Quantification of fractional dynamical stability of EEG signals as a bio-marker for cognitive motor control. *Frontiers in Control Engineering*.

Regalado, A. (2020). *Elon Musk's Neuralink is neuroscience theater*. MIT Technology Review.

Ren, W., & Cao, Y. (2011). *Distributed coordination of multi-agent networks: emergent problems, models, and issues, vol. 1*. Springer.

Riewe, F. (1996). Nonconservative lagrangian and hamiltonian mechanics. *Physical Review E*, *53*(2), 1890.

Rivero, M., Rogosin, S. V., Tenreiro Machado, J. A., & Trujillo, J. J. (2013). Stability of fractional order systems. *Mathematical Problems in Engineering*, *2013*.

Rodgers, A. (2020). *Neuralink Is Impressive Tech, Wrapped in Musk Hype*.

Sabatier, J. (2021). Fractional order models are doubly infinite dimensional models and thus of infinite memory: Consequences on initialization and some solutions. *Symmetry*, *13*(6).

Sabatier, J., Agrawal, O. P., & Machado, J. T. (2007). *Advances in fractional calculus, vol. 4*. Springer.

Sabatier, J., Farges, C., Merveillaut, M., & Feneteau, L. (2012). On observability and pseudo state estimation of fractional order systems. *European Journal of Control*, *18*(3), 260–271.

Safarinejadian, B., Asad, M., & Sadeghi, M. S. (2016). Simultaneous state estimation and parameter identification in linear fractional order systems using coloured measurement noise. *International Journal of Control*, *89*(11), 2277–2296. http://dx.doi.org/10.1080/00207179.2016.1155237.

Safarinejadian, B., Kianpour, N., & Asad, M. (2018). State estimation in fractional-order systems with coloured measurement noise. *Transactions of the Institute of Measurement and Control*, *40*(6), 1819–1835. http://dx.doi.org/10.1177/0142331217691219.

Scalas, E., Gorenflo, R., & Mainardi, F. (2000). Fractional calculus and continuous-time finance. *Physica A: Statistical Mechanics and its Applications*, *284*(1–4), 376–384.

Schalk, G., McFarland, D. J., Hinterberger, T., Birbaumer, N., & Wolpaw, J. R. (2004). BCI2000: A general-purpose brain-computer interface (BCI) system. *IEEE Transactions on Biomedical Engineering*, *51*(6), 1034–1043. http://dx.doi.org/10.1109/TBME.2004.827072.

Schön, T. B., Wills, A., & Ninness, B. (2011). System identification of nonlinear state-space models. *Automatica*, *47*(1), 39–49.

Shah, P., & Agashe, S. (2016). Review of fractional PID controller. *Mechatronics*, *38*, 29–41.

Shahin, A., Ahmed, E., & Omar, Y. A. (2009). On fractional order quantum mechanics. *International Journal of Nonlinear Science*, *8*(4), 469–472.

Shalalfeh, L., Bogdan, P., & Jonckheere, E. A. (2020). Fractional dynamics of PMU data. *IEEE Transactions on Smart Grid*, *12*(3), 2578–2588.

Shlesinger, M. F., Zaslavsky, G. M., & Klafter, J. (1993). Strange kinetics. *Nature*, *363*(6424), 31–37.

Sierociuk, D., & Dzieliński, A. (2006). Fractional Kalman filter algorithm for the states, parameters and order of fractional system estimation. *The International Journal of Applied Mathematics and Computer Science*, *16*(1), 129–140.

Soltan, A., Xia, L., Jackson, A., Chester, G., & Degenaar, P. (2018). Fractional order PID system for suppressing epileptic activities. In *Proceedings 2018 IEEE International Conference Applied System Invention* (pp. 338–341). Chiba, Japan.

Sopasakis, P., & Sarimveis, H. (2017). Stabilising model predictive control for discrete-time fractional-order systems. *Automatica*, *75*, 24–31.

Steyn-Ross, M. L., Steyn-Ross, D. A., & Sleigh, J. W. (2013). Interacting turing-hopf instabilities drive symmetry-breaking transitions in a mean-field model of the cortex: A mechanism for the slow oscillation. *Physical Review X*, *3*(2).

Swerling, P. (1971). Modern state estimation methods from the viewpoint of the method of least squares. *IEEE Transactions on Automatic Control*, *16*(6), 707–719.

Teich, M. C., Heneghan, C., Lowen, S. B., Ozaki, T., & Kaplan, E. (1997). Fractal character of the neural spike train in the visual system of the cat. *Journal of Optical Society of America*, *14*(3), 529–546.

Thurner, S., Windischberger, C., Moser, E., Walla, P., & Barth, M. (2003). Scaling laws and persistence in human brain activity. *Physica A: Statistical Mechanics and its Applications*, *326*(3–4), 511–521.

Tjärnström, F. (1999). *The use of bootstrap in system identification*. Linköping, Sweden: Linköping University Electronic Press.

Torres, D. F., & Malinowska, A. B. (2012). *Introduction to the fractional calculus of variations*. World Scientific Publishing Company.

Trigeassou, J.-C., & Maamri, N. (2011). Initial conditions and initialization of linear fractional differential equations. *Signal Processing*, *91*(3), 427–436.

Turcott, R. G., & Teich, M. C. (1996). Fractal character of the electrocardiogram: Distinguishing heart-failure and normal patients. *Annals of Biomedical Engineering*, *24*(2), 269–293.

Tzoumas, V., Xue, Y., Pequito, S., Bogdan, P., & Pappas, G. J. (2018). Selecting sensors in biological fractional-order systems. *IEEE Transactions on Control of Network Systems*, *5*(2), 709–721.

Valério, D., Trujillo, J. J., Rivero, M., Machado, J. T., & Baleanu, D. (2013). Fractional calculus: A survey of useful formulas. *The European Physical Journal Special Topics*, *222*(8), 1827–1846.

Van Essen, D. C., Smith, S. M., Barch, D. M., Behrens, T. E., Yacoub, E., Ugurbil, K., et al. (2013). The WU-Minn human connectome project: an overview. *Neuroimage*, *80*, 62–79.

Victor, S., Malti, R., Garnier, H., & Oustaloup, A. (2013). Parameter and differentiation order estimation in fractional models. *Automatica*, *49*(4), 926–935.

Victor, S., Melchior, P., Malti, R., & Oustaloup, A. (2016). Robust motion planning for a heat rod process. *Nonlinear Dynamics*, *86*(2), 1271–1283.

Vinagre, B. M., & Calderón, A. J. (2006). On fractional sliding mode control. In *Proceedings 7th Portuguese Conference Automatic Control*.

Vinagre, B., Podlubny, I., Hernandez, A., & Feliu, V. (2000). Some approximations of fractional order operators used in control theory and applications. *Fractional Calculus & Applied Analysis*, *3*(3), 231–248.

Wang, J., Niebur, E., Hu, J., & Li, X. (2016). Suppressing epileptic activity in a neural mass model using a closed-loop proportional-integral controller. *Scientific Reports*, *6*.

Wei, Y., Chen, Y., Wang, J., & Wang, Y. (2019). Analysis and description of the infinite-dimensional nature for nabla discrete fractional order systems. *Communications in Nonlinear Science and Numerical Simulation*, *72*, 472–492.

Wei, W., Wei, X., Xia, P., Zuo, M., & Shen, D. (2019). Seizure control by a learning type active disturbance rejection approach. *IEEE Access*, *7*, 164792–164802.

Wei, W., Wei, X., & Zuo, M. (2019). Control of epileptiform waves in a neural mass model. In *Proc. 2019 Chin. control conf.* (pp. 6860–6864). Guangzhou, China.

Wei, W., Wei, X., Zuo, M., Yu, T., & Li, Y. (2019). Seizure control in a neural mass model by an active disturbance rejection approach. *International Journal of Advanced Robotic Systems*, *16*(6), 1–15.

Wendling, F., Bellanger, J.-J., Bartolomei, F., & Chauvel, P. (2000). Relevance of nonlinear lumped-parameter models in the analysis of depth-EEG epileptic signals. *Biological Cybernetics*, *83*(4), 367–378.

Wendling, F., Benquet, P., Bartolomei, F., & Jirsa, V. (2016). Computational models of epileptiform activity. *Journal of Neuroscience Methods*, *260*, 233–251.

Werner, G. (2010). Fractals in the nervous system: Conceptual implications for theoretical neuroscience. *Frontiers Physiology*, *1*.

West, B. J. (2014). Colloquium: Fractional calculus view of complexity: A tutorial. *Reviews of Modern Physics*, *86*(4), 1169.

West, B. J. (2016). *Fractional calculus view of complexity: tomorrow's science*. Boca Raton, FL, USA: CRC Press.

West, B. J., Turalska, M., & Grigolini, P. (2015). Fractional calculus ties the microscopic and macroscopic scales of complex network dynamics. *New Journal of Physics*, *17*(4), Article 045009.

West, B. J., Turalska, M., & Grigolini, P. (2016). *Networks of echoes*. Cham, Switzerland: Springer International Publishing AG.

Willems, J. C. (2004). Deterministic least squares filtering. *Journal of Econometrics*, *118*(1–2), 341–373.

Wu, C., Yang, C., Zhao, H., & Zhu, J. (2016). On the convergence of the EM algorithm: A data-adaptive analysis. arXiv:1611.00519.

Xia, L., Soltan, A., Zhang, X., Jackson, A., Tessier, R., & Degenaar, P. (2019). Closed-loop proportion-derivative control of suppressing seizures in a neural mass model. In *Proc. 2019 IEEE Int. symp. circuits and syst.* (pp. 1–5). Sapporo, Japan.

Xue, Y., & Bogdan, P. (2017). Constructing compact causal mathematical models for complex dynamics. In *Proceedings of the 8th International Conference on Cyber-Physical Systems* (pp. 97–107). Pittsburgh, PA, USA.

Xue, Y., Pequito, S., Coelho, J. R., Bogdan, P., & Pappas, G. J. (2016). Minimum number of sensors to ensure observability of physiological systems: A case study. In *Proceedings 54th Annual Allerton Conference Communication, Control, and Computing* (pp. 1181–1188). Monticello, IL, USA.

Xue, Y., Rodriguez, S., & Bogdan, P. (2016). A spatio-temporal fractal model for a CPS approach to brain-machine-body interfaces. In *Proceedings of the 2016 Design, Automation & Test in Europe Conference & Exhibition* (pp. 642–647). Dresden, Germany.

Yan, B., Yin, M., & Sarkar, P. (2017). Convergence of gradient EM on multi-component mixture of Gaussians. In *Advances in Neural Information Processing Systems* (pp. 6956–6966). Long Beach, CA, USA.

Zaky, M. A., & Machado, J. T. (2017). On the formulation and numerical simulation of distributed-order fractional optimal control problems. *Communications in Nonlinear Science and Numerical Simulation*, *52*, 177–189.

Zames, G., & Owen, J. (1993). A note on metric dimension and feedback in discrete time. *IEEE Transactions on Automatic Control*, *38*(4), 664–667.

Zhang, X., & Chen, Y. (2012). Remarks on fractional order control systems. In *2012 American Control Conference* (pp. 5169–5173). IEEE.

Zitane, H., Boutoulout, A., & Torres, D. F. (2020). The stability and stabilization of infinite dimensional Caputo-time fractional differential linear systems. *Mathematics*, *8*(3).